An Environmental Restriction impairs HIV-1 virion fusion and triggers innate immune recognition

Samy Sid Ahmed[a]**, Liv Zimmerman**[b]**, Andrea Imle**[a]**, Katrin Wuebben**[c]**, Nadine Tibroni**[a]**, Lena Rauch-Wirth**[d]**, Jan Münch**[d]**, Petr Chlanda**[b]**, Frederik Graw**[c,f,g] **and Oliver T. Fackler**[a,e]#

[a] Department of Infectious Diseases, Integrative Virology, CIID, Heidelberg University, Medical Faculty Heidelberg, Heidelberg, Germany

[b] Schaller Research Groups, Department of Infectious Diseases, Virology, Heidelberg University, Medical Faculty Heidelberg, 69120 Heidelberg, Germany

[c] BioQuant-Center for Quantitative Biology, Heidelberg University, 69120 Heidelberg, Germany

[d] Institute of Molecular Virology, Ulm University Medical Center, 89081 Ulm, Germany

[e] German Centre for Infection Research (DZIF), Partner Site Heidelberg, Germany

[f] Interdisciplinary Center for Scientific Computing, Heidelberg University, 69120 Heidelberg, Germany

[g] Friedrich-Alexander-Universität Erlangen-Nürnberg, Department of Medicine 5, 91054 Erlangen, Germany

Running title: TLR sensing by extracellular matrix

Corresponding author at:

Department of Infectious Diseases, Integrative Virology, University Hospital Heidelberg, Im Neuenheimer Feld 344, 69120 Heidelberg, Germany Phone: ++49-(0)6221-561322; Fax: ++49-(0)6221-565003; Email: oliver.fackler@med.uni-heidelberg.de

Abstract

In vivo, HIV-1 replicates within 3D tissues, yet the impact of tissue-like environments on viral spread is largely unknown. Our previous research identified that synthetic 3D environments impose an *Environmental Restriction to cell-free Virus Infectivity* (ERVI) that diminishes HIV-1 particle infectivity. Here, mechanistic studies reveal that ERVI is implemented within minutes, saturable and induced by different adhesive tissue-like 3D matrices. ERVI reduces infectivity across a wide range of primary HIV-1 strains and virions bearing distinct viral glycoproteins but does not damage virion morphology or affect their binding to target cells. Rather, ERVI impairs virion fusion with target cells and infectivity enhancing peptide nanofibrils can restore efficient infection. In addition, ERVI sensitizes HIV-1 particles for recognition by monocyte-derived macrophages via toll-like receptors 4 and 8, triggering pronounced pro-inflammatory cytokine secretion. These results suggest that ERVI represents a broadly acting, tissue-intrinsic barrier to virus spread that reduces the fusogenicity of cell-free virions and sensitizes them for innate immune recognition.

Key words: HIV-1, tissue-like 3D environments, collagen, virion infectivity restriction, innate immune sensing

Introduction

Many viruses including Human Immunodeficiency Virus (HIV) can spread from infected donor cells either by the release of cell-free particles into the extracellular space that then diffuse to new target cells (cell-free transmission) or via close physical contacts between donor and target cell (cell-associated transmission) (Hubner *et al*, 2009; Jolly *et al*, 2004; Phillips, 1994). In the case of HIV, cell-associated transmission occurs at highly polarized cell-cell contacts referred to as virological synapse and in cell culture models, this transmission mode is significantly more efficient than infections by cell-free virus particles (Dimitrov *et al*, 1993; Iwami *et al*, 2015; Kolodkin-Gal *et al*, 2013; Sourisseau *et al*, 2007). Virological synapses have been documented in small animal models for HIV but also murine leukemia virus (Murooka *et al*, 2012; Sewald *et al*, 2015), but which transmission mode predominates in infected tissue remained unclear. To start addressing this problem, we previously established three dimensional (3D) collagen matrices as a tissue-like cell culture model in which parameters such as cell density and 3D organization can be controlled (Ahmed *et al*, 2020; Imle *et al*, 2019). At conditions of limited cell density where virions either need to diffuse or donor cells have to migrate to new target cells to sustain HIV spread, computational modelling and subsequent experimental validation identified cell-associated transmission as the predominant mode of virus spread in 3D collagen. Under such conditions, motility was found to be a relevant parameter for target cells' permissivity for infection (Lopez *et al*, 2022). In contrast, in 3D collagen with very high cell density or in classical suspension cultures, cell-free and cell-associated transmission modes supported HIV-1 spread with comparable efficacy. This shift towards cell-associated virus transmission in tissue-like environments reflected an enhanced efficiency of cell-associated spread, but also a significant reduction of the infectivity of HIV-1 particles. Imaging analysis revealed that HIV-1 particles freely diffuse in the tissue-like environment but undergo short (milliseconds) and reversible physical interactions with collagen fibers. These findings suggested that in tissue, the physical

71   contact with extracellular matrix limits the infectivity of cell-free HIV-1 particles. In analogy

72   to intracellular barriers that counteract HIV-1 spread, such as host cell restriction factors as

73   part of the cell intrinsic immune system, we refer to this tissue intrinsic phenomenon as

74   *Extracellular Restriction of Virion Infectivity* (ERVI).

75   As an enveloped virus particle, the infectious potential of HIV-1 virions is determined by a

76   large number of parameters. This comprises basic properties such as particle integrity,

77   packaging of the viral genome and essential enzymes, incorporation of the viral glycoprotein

78   Env, and liquid-order membrane microdomain-like lipid composition of the viral envelope

79   (Brügger *et al*, 2006; Nieto-Garai *et al*, 2021; Sáez-Cirión *et al*, 2002; Yi *et al*, 2006).

80   Reflecting this complex set of requirements for the generation of an infectious HIV particle, a

81   wide range of cellular restriction factors including tetherin, SERINC proteins, 90K, IFTIM

82   proteins, GBP 2 and 5 and PSGL-1 reduce HIV-1 infectivity via distinct mechanisms (Braun

83   *et al*, 2019; Krapp *et al*, 2016; Liu *et al*, 2019; Lodermeyer *et al*, 2013; Neil *et al*, 2008; Rosa

84   *et al*, 2015; Usami *et al*, 2015; Venkatesh & Bieniasz, 2013). In this study, we set out to gain

85   more insight into the mechanism and functional consequences of ERVI.

86

87

Results

ERVI is a rapidly induced, saturable and conserved restriction to HIV-1 infectivity

Our previous results had established that tissue-like 3D collagen environments pose the ERVI barrier that markedly reduces the infectivity of HIV-1 particles recovered from the supernatant of 3D collagen matrices in which virus producing cells or cell-free virus particles had been embedded (Imle *et al.*, 2019). Single particle tracking revealed that HIV virions diffuse freely in the 3D matrix but undergo physical contacts with collagen fibers. These interactions were transient in the millisecond range and did not result in coating of the fibers with virus particles (Imle *et al.*, 2019). Since physical stress can impair virus infectivity by inducing shedding of the viral glycoprotein from the virion, and the efficacy of glycoprotein incorporation is an important determinant of infectivity (Chertova *et al*, 2002; Day *et al*, 2004) we first tested if contact with 3D collagen alters the amounts of the HIV-1 glycoprotein Env in these particles. However, Env protein levels were comparable between virions cultured in suspension or in 3D collagen (EV 1A, B). To gain more insight into the nature of ERVI, we conducted a kinetic analysis and compared the impact of culturing HIV-1 NL4.3 particles in suspension or in 3D collagen with different densities (dense: 3 mg/ml; loose: 1.6 mg/ml) (Fig. 1A). Virion infectivity was assessed on Tzm-bl reporter cells, in which the luciferase gene is under control of the HIV-1 promoter and de novo expression of the viral transactivator Tat in productively infected cells triggers luciferase expression. The amount of luciferase expression relative to the amounts of virus used for infection, as determined by quantifying the activity of viral reverse transcriptase by the SG-PERT assay, yielded the relative infectivity of HIV particles. In line with our previous findings, single rounds of infection revealed that culturing HIV-1 in dense or loose 3D collagen for 16h reduced their infectivity to 10.6% or 14.3% of the particles from parallel suspension cultures (Fig. 1B). Kinetic analysis revealed that infectivity was reduced immediately or within 4h after contact with dense 3D collagen in

113   dense and loose collagen, respectively. The subsequent reduction of the remaining virion

114   infectivity over time followed comparable kinetics under all culture conditions (Fig. 1C).

115   To assess how conserved the sensitivity to ERVI is among primary lentiviruses, we

116   next analyzed the impact of 3D collagen on a panel of lab-adapted and primary HIV-1 strains

117   as well as one HIV-2 strain on Tzm-bl reporter cells (Fig. 1D). The results revealed that the

118   infectivity of all HIV strains tested was significantly reduced by ERVI, but to varying

119   magnitude ranging from strong (52.9 fold, HIV-1 ADA, dense collagen) to very mild

120   inhibition (1.6 fold, HIV-1 RHGA, loose collagen). The reduction of infectivity by ERVI was

121   independent of the HIV-1 entry co-receptor preference but patient-derived transmitted

122   founder and chronic HIV-1 variants tended to be less sensitive to ERVI than lab-adapted

123   HIV-1. Notably, also HIV-1 virions lacking Env but pseudotyped with the glycoprotein of

124   vesicular stomatitis virus (VSVG) were sensitive to ERVI. To analyze further the impact of

125   the viral glycoprotein for the sensitivity to ERVI, we pseudotyped GFP encoding lentiviral

126   particles with the unrelated glycoproteins of the HCV isolates Con1 or JFH1 and tested their

127   infectivity on Huh 7.5 cells by flow cytometry-based quantification of GFP expressing cells

128   (Fig. 1E). While the infectivity of these virions was also reduced, the effects were moderate

129   and only reached statistical significance for particles pseudotyped with JFH1 glycoprotein in

130   dense collagen. The analysis of lentiviruses pseudotyped with the Influenza HA or the Ebola

131   virus glycoproteins was not informative since already 16h culture in suspension reduced the

132   infectivity of these particles below the detection limit (EV 1C,D). Together, these results

133   suggest that the viral glycoprotein is a key determinant for the sensitivity to ERVI. Reduction

134   of virus infectivity is observed with glycoproteins of different receptor specificity and

135   topology but type I (HIV) and type III (VSVG) glycoproteins may be more sensitive to ERVI

136   than type II glycoproteins (HCV).

137   Since cellular restrictions to virus infection typically act as physical barriers that can

138   be overcome by an excess of virus particles, we analyzed if the amounts of virions added to a

6

139   constant culture volume affected the magnitude of reduction in virion infectivity (Fig. 1F).

140   While the relative infectivity of virus particles in suspension was unaffected by the

141   concentration of virus, the infectivity reduction by ERVI was significantly less efficient at

142   higher virus concentrations in dense or loose collagen (Fig. 1F; relative infectivity 7- or 2-fold

143   higher at 10^7 vs. 10^5 BCUs in dense or loose collagen; $p<0.09$ and $p<0.015$ respectively).

144   We next sought to define how the architecture and biophysical properties of the 3D

145   matrix affect its ability to reduce the infectivity of HIV-1 virions and compared several

146   matrices that (i) can be polymerized without harming *per se* the infectivity of HIV particles

147   (e.g. high temperature or UV exposure) and (ii) result in pore size that allows HIV-1 particles

148   to diffuse within and out of the 3D matrix (Fig. 1G, EV 1E). The dense and loose collagen

149   matrices are assembled into fibers polymerized from purified type I collagen proteins, the

150   most abundant collagen type in tissue. Confocal reflection microscopy analysis of these

151   matrices confirmed the different density of both types of type I collagens after polymerization

152   and revealed that the dense collagen was enriched in branched collagen bundles (EV 1E).

153   Similarly, the architecture of 3D matrices made of type III collagen, the second most

154   abundant fibrillary collagen in tissue that is synthesized by reticular cells and lines e.g.

155   vasculature, resembled that of dense collagen, albeit with shorter and thinner collagen

156   bundles, and type III collagen reduced HIV-1 infectivity with similar efficacy. We also tested

157   Matrigel, a complex extracellular environment of the basal membrane rich in collagen I as

158   model for type I collagen fibers in a complex tissue environment. Matrigel assembles into 3D

159   matrices with higher pore sizes and heterogeneity than purified collagen matrices (Anguiano

160   *et al*, 2020). Although matrigel displayed a punctate morphology, its antiviral activity was

161   comparable to that of dense collagen (24.1+/- 4.4% of suspension or 4-fold reduction). In

162   contrast, agarose hydrogels, which are made of bundles of linear filaments without cell

163   adhesion features, did not impair the infectivity of HIV-1 virions.

164   Together, these results reveal that a broad range of HIV-1 variants are sensitive to

165   ERVI. This extracellular restriction is exerted rapidly upon contact with the 3D environment,

166   can be saturated by excess of virus particles, and is exerted by a variety of adhesive

167   extracellular matrix components.

168

169   **ERVI restricts HIV-1 infectivity without affecting structural integrity of virus particles**

170   We next addressed in more detail how the physical contact of HIV particles with the 3D

171   collagen environment affects their infectivity. We considered the possibility that following

172   transient contacts of HIV-1 particles with collagen fibers, collagen material remains attached

173   to the virions and compromises their infectivity. Embedding of HIV-1 particles in

174   fluorescently labelled collagen (EV 2A), which exerted ERVI with similar efficacy than non-

175   labelled collagen (Fig. 2A), resulted in a small population of fluorescent HIV-1 particles

176   (8.5+/-4.7 %, Fig. 2B, C). However, these events were not frequent enough to explain the

177   over 10-fold reduction in infectivity observed. To assess potential physical damage of the

178   virions, we next analyzed their morphology by cryo-electron tomography. HIV-1 particles

179   kept in suspension or in dense or loose 3D collagen were placed on EM grids and processed

180   for cryo-ET analysis. Under all three conditions, enveloped HIV-1 particles with the typical

181   conical core and a diameter ranging from 104 to 154 nm (mean values: suspension: 134.5+/-

182   11.5 nm, dense: 135.2 +/- 9.6nm, loose: 132.0 +/- 11.6 nm) were observed (Fig. 2D, E). All

183   analyzed particles appeared intact without appreciable membrane rupture or deformation and

184   showed sparsely distributed Env spikes. We did not observe aberrations in HIV-1 particle

185   architecture resulting from the interaction with 3D collagen. As size comparison, we also

186   analyzed the morphology of dense and loose collagen fibers, which displayed the

187   characteristic structure of collagen fibrils, with a tight packing of D-periodic polyproline type

188   II helices corresponding to the spacing between individual tropocollagen monomers

189   (Shoulders & Raines, 2009) (Fig. 2F, EV. 2B). However, none of the images obtained for

190   HIV particles displayed virion-associated material reminiscent of collagen fibers (Fig. 2D),

191   suggesting that the detection of fluorescent HIV particles after contact with fluorescent 3D

192   matrices may reflect the transfer of fluorescent dye rather than collagen material. Of note,

193   incubating HIV-1 particles with the peptide EF-C or RM-8, which boost the infectivity of

194   HIV-1 particles by enhancing their interaction with target cells (Rauch-Wirth L *et al*, 2023;

195   Yolamanova *et al*, 2013), increased the infectivity of all particles and almost fully overcame

196   the inhibitory effect of ERVI (Figs. 2G, H). Together, these results reveal that ERVI does not

197   result from global disruption of HIV-1 particle architecture and suggest that ERVI does not

198   affect the intrinsic replication potential of HIV particles but rather the efficacy of their

199   interaction with target cells.

200

201   **ERVI is manifest at the step of virus fusion to TZM-bl reporter cells without affecting**

202   **virion binding to target cells**

203   The finding that infection enhancers boost the infectivity of HIV-1 particles subject to ERVI

204   suggested that ERVI acts at the early step of the viral life cycle. To test if ERVI impairs the

205   ability of HIV-1 particles to bind to target cells, we generated virions that incorporated

206   Vpr.mRuby2 during virus production for visualization (Gallucci *et al*, 2023) (Fig. 3A).

207   Incorporation of Vpr.mRuby2 did not affect their sensitivity to infectivity reduction upon

208   contact with 3D collagen (Fig. 3B). To visualize their interaction with the surface of Tzm-bl

209   target cells by spinning disk microscopy, cells were incubated with virus particles for 2h at

210   4°C to avoid particle internalization and to detect individual fluorescent HIV-1 particles

211   attached to the cell surface (Fig. 3C, EV 3). While incubating these particles for 16 h in

212   suspension slightly reduced the number of virions detected at the surface of target cells (Fig.

213   3D, 2 +/- 0.5 bound virus particles/cell for fresh virus vs. 1.1 +/- 0.4 bound virus particles/cell

214   for suspension), no additional reduction in binding efficacy was observed for virions that had

215   been embedded in dense or loose 3D collagen. Notably however, prior contact with dense 3D

9

216 collagen resulted in significantly larger aggregates of virus particles at the surface of target

217 cells. Such particle aggregation was not observed upon contact with loose collagen, indicating

218 that this effect is not essential for ERVI. The predominant action of ERVI therefore is not at

219 the level of virus binding to target cells.

220 To assess the ability of HIV particles to fuse with target cells membranes, Vpr.Blam

221 containing particles were produced and used to measure the conversion of the ß-lactamase

222 (BLAM) substrate CCF2 to the cytosol of target cells by flow cytometry as a measure for

223 fusion (Cavrois *et al*, 2002; Gallucci *et al.*, 2023). The incorporation of Vpr.Blam did not

224 affect the sensitivity of the virions to ERVI in dense collagen, while the infectivity reduction

225 by loose collagen was slightly less pronounced (Fig. 4B). Analyzing the fusion capacity of

226 these particles revealed efficient cytosolic delivery of Vpr.Blam by HIV-1 particles kept in

227 suspension (10.4 +/- 2.4%), which was dependent on the viral glycoprotein Env and could be

228 inhibited by the HIV fusion inhibitor T20 (Fig. 4C, D). This fusion capacity was strongly

229 impaired for particles that had prior contact with dense 3D collagen (1.5 +/- 0.7 %). Loose

230 collagen (5.4 +/- 2.5%) had a less pronounced effect on the fusion capacity of HIV-1 particles

231 and overall, infection rates and fusion capacity under the different conditions analyzed were

232 moderately correlated (Fig. 4E). We conclude that the interaction of HIV-1 particles with

233 tissue-like environments reduces their infectivity by impairing their ability to fuse with target

234 cells and that ERVI may also affect additional post entry steps.

235

236 **ERVI moderately reduces infection of primary CD4+ T cells and MDMs**

237 HeLa-derived Tzm-bl cells are a convenient and widely used reporter cell to quantify the

238 infectivity of HIV-1 particles but cannot reflect the differences in entry binding and receptor

239 densities, membrane lipid composition as well as uptake pathways between different primary

240 target cells (Choudhry *et al*, 2006).We therefore sought to analyze the relevance of ERVI for

241 HIV-1 infection of primary human CD4 T cells and primary human monocyte-derived

10

242 macrophages (MDMs). To be able to use this analysis with the same virus, we employed a

243 HIV-1 variant that uses CCR5 as entry coreceptor (HIV-1 NL4.3 R5) (Fig. 5A). This co-

244 receptor tropism did not affect the sensitivity of these particles to ERVI when assessed on

245 Tzm-bl cells (Fig. 5B), which was again more pronounced in dense than loose collagen.

246 Productive infection of primary target cells was assessed by quantifying the number of cells

247 with intracellular p24 capsid by flow cytometry (CD4 T cells, Fig. 5C, MDMs, Fig. 5D). The

248 reverse transcriptase inhibitor efavirenz (EFZ) was used to define background detection of

249 input virus. On both CD4 T cells and MDMs, productive infection by particles with prior

250 contact to dense 3D collagen was significantly reduced (3.6-fold reduction to 27.5% of

251 suspension on CD4 T cells, 2.9-fold reduction to 34.8% of suspension on MDMs) and loose

252 collagen only mediated a very mild reduction that did not reach statistical significance (1.8-

253 fold on CD4 T cells, 1.4-fold on MDMs). These results reveal that ERVI reduces the

254 infectivity of cell-free HIV-1 particles on primary target cells, albeit with lower efficacy than

255 on e.g. TZM-bl cells.

256   With 27.5% infectivity remaining, the impact of ERVI on infection of primary CD4 T

257 cells was less pronounced than on Tzm-bl cells, where ERVI reduces virion infectivity to 14%

258 of that of virions in suspension culture. Our computational model of HIV-1 replication in 3D

259 collagen cultures of primary human mononuclear cells, which predicted that cell-associated

260 virus transmission largely dominates over cell-free infection in 3D collagen matrices (Imle *et

261 al.*, 2019), was based on the value of 14% of cell-free infectivity remaining in 3D. We

262 therefore asked if the fact that the infectivity of these virions is higher on the primary target

263 cells present in these 3D cultures affects this conclusion. To this end, we revisited our

264 previous analyses estimating the efficacy of cell-free and cell-to-cell transmission within

265 suspension and 3D collagen matrices by mathematical modelling (Imle *et al.*, 2019). Varying

266 the parameter defining the reduced infectivity of cell-free infection within collagen compared

267 to suspension, we estimate that the contribution of cell-free transmission to viral transmission

11

268 within collagen continuously increases with increasing infectivity preservation (Fig. 5E).

269 Differences between estimates for loose and dense collagen are partly affected by technical

270 compensations within the fitting procedure due to model constraints, which lead to reduced

271 estimates of cell-to-cell transmission rates within dense collagen and thereby potentially

272 underestimating the contribution of cell-to-cell transmission for this environment (EV 4C).

273 Under these conditions, the best estimates predict that an infectivity reduction to 27.5%

274 results in a contribution of cell-cell transmission to overall virus spread of 60% and 30% in

275 loose and dense collagen, respectively. We conclude that in our primary cell 3D cultures, cell-

276 associated transmission remains an important driver of HIV-1 spread in 3D collagen even if

277 the infectivity of cell-free particles is less reduced than previously thought.

278

279 **ERVI sensitizes virus particles for TLR-mediated recognition by MDMs**

280 We tested next if ERVI has functional implications in MDMs in addition to reducing virion

281 infectivity. Since MDMs can exhibit efficient innate immune reactions to challenge with HIV

282 particles (Pierini *et al*, 2021; Rasaiyaah *et al*, 2013; Yin *et al*, 2020), we quantified the

283 amounts of a panel of cytokines in the supernatant of MDMs 3 days after challenge with HIV-

284 1 particles kept in suspension or in 3D collagen. Interestingly, prior encounter of HIV-1

285 particles with tissue-like 3D environments markedly and broadly altered the cytokine

286 response of MDMs, resulting in increased release of important pro-inflammatory cytokines

287 such as IL-6, IL-8 and TNFα but also G-CSF, GM-CSF, GROα, IL-17, IP-10, MCP-3,

288 CXCL9 and MIP-1α/β (Fig. 6B, compare suspension vs. dense and loose collagen). To gain

289 insight into the HIV replication intermediate as well as the MDMs sensors that respond to

290 HIV-1 particles subjected to ERVI, we challenged MDMs with HIV-1 particles derived from

291 suspension or dense collagen cultures in the presence of selective inhibitors (Fig. 6C).

292 Interestingly, interfering with virus fusion by the entry inhibitor T20 or with reverse

293   transcription by efavirenz (EFZ) did not impair the ERVI-mediated increase in the secretion

294   of IL-6 or IL-8 (EV 5A). Entry and early post-entry steps of the HIV-1 life cycle are thus not

295   required for ERVI-mediated induction of pro-inflammatory cytokine production, suggesting

296   that innate recognition occurs in the context of non-productive uptake of virus particles. In

297   line with this scenario, inhibition of the cytoplasmic DNA sensor cGAS had no effect on the

298   ERVI-mediated induction of IL-6 or IL-8 secretion. Similarly, pharmacological inhibition

299   suggested that toll-like receptors (TLR) 1/2, 3 and 9 are not involved in the recognition of

300   ERVI-treated HIV particles. In contrast, inhibiting the endosomal TLR-8 that recognizes

301   single stranded RNA (Heil *et al*, 2004), or TLR-4, which recognizes bacterial

302   lipopolysaccharide (LPS) but also viral proteins (Del Cornò *et al*, 2016), or the TLR signaling

303   adaptor MyD88 (Medzhitov *et al*, 1998) fully abrogated the induction of IL-6 production by

304   ERVI-treated HIV-1 (Fig. 6C). Inhibition of TLR-8 or MyD88, but not of TLR-4, also

305   decreased the release of IL-8 by MDMs after challenge with collagen cultured virions (EV

306   5A). Collectively, these results reveal that ERVI sensitizes HIV-1 particles for recognition by

307   TLR-8 and -4 in the context of non-productive uptake of HIV-1 particles by MDMs.

Discussion

Tissue-like environments shape the mode of HIV-1 spread towards cell-associated transmission by optimizing duration and architecture of cell-cell contacts but also by suppressing the infectivity of cell-free virus particles. Investigating the mechanism and relevance of this intrinsic antiviral property of extracellular environments, ERVI, defined that this restriction affects the function of a broad range of viral glycoproteins and impairs fusion but not binding of cell-free virus particles with target cells. Glycoprotein incorporation and virion morphology are unaffected by ERVI and the restriction can be overcome by using infectivity enhancing peptide nanofibrils, suggesting that ERVI acts directly on the fusogenicity of the glycoprotein. This may involve modification of glycoprotein conformation and/or lipid microenvironment that result from the short physical interaction of virions with the 3D matrix and may affect the positioning of the glycoprotein in the viral membrane or their ability to cluster for efficient receptor interactions (Boesze-Battaglia *et al*, 1996; Chojnacki *et al*, 2012; Watala *et al*, 2002). Viral glycoproteins with differing sensitivity to ERVI will provide valuable tools for futures studies into the molecular mechanism of the impairment of Env function by ERVI.

Assessing the impact of ERVI on MDM target cells revealed a functional consequence of this extracellular restriction in addition to reducing virion infectivity: HIV particles that underwent prior contact with tissue-like environments triggered innate immune recognition resulting in the production of proinflammatory cytokines. Since infection rates of ERVI-treated HIV particles do not correlate with cytokine production and blocking infection does not abrogate sensing, ERVI-induced innate sensing of HIV particles does not occur during productive infection. Rather, the reduced ability to fuse with target cells is likely associated with increased recognition of particles in a non-productive uptake pathway by TLR-8 and at the cell surface by TLR-4. Since most HIV particles are subject to non-productive endocytic

333 uptake already in the absence of ERVI (Fackler & Peterlin, 2000; Maréchal *et al*, 1998;

334 Maréchal *et al*, 2001; Schaeffer *et al*, 2004), we hypothesize that ERVI enhances innate

335 immune recognition by sorting of particles into an uptake pathway particularly prone to TLR-

336 8 recognition (Fig. 7). TLR8-mediated sensing of HIV-1 genomes has been reported in a

337 variety of cell systems and is associated with improved control of HIV replication in patients,

338 the regulation of latency, and can be exploited by HIV to allow the productive infection of

339 plasmacytoid dendritic cells (Gringhuis *et al*, 2010; Li *et al*, 2023; Meås *et al*, 2020; Oh *et al*,

340 2008). The role of TLR-4, which recognizes LPS but also viral proteins at the cell surface

341 (Chow *et al*, 1999), in HIV-1 infection is less established. However, R5-tropic HIV-1 Env

342 (Env), Vpr and Tat proteins have been reported to trigger TLR-4 signaling (Bahraoui *et al*,

343 2020; Del Cornò *et al.*, 2016; Hoshino *et al*, 2010) and in particular for the recognition of

344 Env, ERVI may potentiate this effect. Increased innate immune recognition is also associated

345 with the reduction of virion infectivity by the host cell factor SERINC5 (Pierini *et al.*, 2021)

346 and the capacity of dendritic cells to adapt to tissue-like environments (Gallucci *et al.*, 2023).

347 Regulation by the extracellular environment thus emerges as an important parameter for

348 innate immune responses to HIV-1 infection.

349 Our previous computational analysis had identified cell-associated infection as the

350 predominant HIV-1 transmission mode in 3D cultures (Imle *et al.*, 2019). This conclusion was

351 based on virion infectivity quantifications on model cell lines and was now questioned by our

352 experimental finding that the effect of ERVI on infection of primary human CD4 T cells is

353 less pronounced. Varying the magnitude of infectivity impairment in the model however

354 revealed that even at these lower levels of cell-free infectivity reduction, cell-associated

355 infection remains an important transmission mode. This relevant role of cell-associated

356 transmission likely reflects that the long diffusion times required for virions to reach new

357 target cells in 3D matrices are associated with significant reduction in their infectivity. This in

15

358 turn raises the question why the production of large amounts of cell free virus particles is

359 maintained in lentiviral evolution. The sensitization of non-infectious particles for the

360 induction of pro-inflammatory cytokine responses by extracellular matrix identified in this

361 study may be one reason since cytokines such as TNF-α, IL-2, IL-1 and IL-6 can increase the

362 permissiveness of primary target cells to HIV-1 infection (Foli *et al*, 1995; Maréchal *et al*,

363 1999; Poli *et al*, 1994; Vyakarnam *et al*, 1990). Although the infection rates of local target

364 cells are reduced by ERVI, the induced innate recognition may create a replication-prone

365 tissue microenvironment and thereby indirectly facilitate virus spread in tissue. ERVI is

366 exerted by 3D collagen from different species that form fibers of distinct architectures,

367 suggesting that this restriction can be relevant in different HIV target tissues. Notably, chronic

368 immune activation and inflammation observed in HIV patients even under therapy is

369 associated with lymph node fibrosis, which is thought to contribute to HIV pathogenesis

370 (Estes, 2013). Fibrosis reflects the deposition of large amounts of collagen with altered

371 structural and biophysical properties (Jones *et al*, 2018), which may also impact its antiviral

372 ERVI activity. Collectively, our study suggests that the reduction of virus particle infectivity

373 coupled to their enhanced innate immune recognition constitutes a tissue-intrinsic antiviral

374 immune mechanism. Future studies will focus on the role of ERVI in different fibrotic and

375 non-fibrotic target tissues as well as in the context of virus-host evolution.

376

Limitations:

378 Our study employed various 3D matrices to define the properties of tissue-like environments

379 to suppress HIV particle infectivity but this does not assess directly if HIV-1 particles

380 generated in human tissue are subjected to ERVI. This could in principle be tested with HIV-1

381 particles derived from organotypic explants models, e.g. tonsil or cervix. However, it is

382 impossible to ensure that particles produced in such cultures were really produced in densely

383   packed tissue areas and underwent physical contact with tissue fibers. While both dense and

384   loose collagen exert ERVI, the restriction is less pronounced for loose collagen and further

385   mechanistic studies will be required to define the molecular basis for this difference.

17

Materials and Methods:

Cells. 293T cells (ATCC, CRL-3216) and TZM-bl reporter cells (courtesy of NIH AIDS Reagent Program (ARP-8129)) were cultured in Dulbecco's Modified Eagle's Medium (DMEM, Gibco) supplemented with 10% heat-inactivated fetal calf serum (FCS, Capricorn) and 1% penicillin/streptomycin (Gibco). Huh 7.5 cells were maintained in complete DMEM medium supplemented with non-essential amino acids.

Primary CD4+ T cells and MDMs. Human peripheral blood of healthy, HIV-negative donors was obtained from the blood bank HD, according to regulation by local ethics committee (S-024/2022). CD4 T cells were isolated from human peripheral blood of healthy, HIV-negative donors using the RosetteSep Human CD4 T cell enrichment kit (StemCell Technologies) according to the manufacturer's protocol. The cells were then activated with Dynabead Human T-Activator CD3/CD28 (Gibco), or in a 3x3 activation as described previously (Imle *et al.*, 2019)rd

for 72h and cultured in Roswell Park Memorial Institute Medium (RPMI, Gibco) supplemented with 10% heat-inactivated FCS, 1% penicillin–streptomycin, and 10 ng/ml interleukin 2 (IL-2, Biomol). To generate monocyte-derived macrophages (MDMs), peripheral blood mononuclear cells (PBMCs) were isolated from buffy coats by Biocoll (Merck Biochrom) density gradient centrifugation. CD14$^+$ monocytes were then isolated from PBMCs by positive selection using magnetic beads (CD14 MicroBeads; Miltenyi Biotech) and an AutoMACS Pro Separator (Miltenyi Biotech). $1x10^5$ monocytes per well were then seeded in glass-bottom 96 well plates that were previously coated with fibronectin (2 µg/cm²) and maintained at 37°C with 5% CO_2 in complete RPMI in the presence of 5% human AB serum (Sigma-Aldrich) for differentiation into MDMs for 10-14 day (Pierini *et al.*, 2021).

18

412 **Viruses.** Virus stocks of replication competent HIV-1 and HIV-2 strains (pNL4.3 WT,

413 pNL4.3 Δnef, pNL4.3 R5, ADA, CH077, CH0 58.c, CH0198, RHGA, CH0167, CH0293,

414 HIV-2 Rod9-GFP) were generated by transfecting 293T cells (sub-confluent 15cm² dishes)

415 with 25 μg of proviral constructs alongside 75 μl of linear polyethyleneimine (PEI, Sigma

416 Aldrich) in Optimem medium (Gibco). Viruses containing Vpr-BlaM and Vpr-mRuby2 were

417 similarly produced by PEI co-transfection of 293T cells using 25 μg of pNL4.3 provirus with

418 7.5 μg of Vpr fusion constructs. For single round HIV-1 virus production (pNL4.3 Δenv

419 VSVg, pNL4.3 Δenv HIV-1 Env), 22μg of pNL4.3 Δenv were used, complemented with 3 μg

420 of the respective glycoprotein expression vectors (Gallucci *et al.*, 2023; Pierini *et al.*, 2021).

421 Two to three days post transfection, supernatants were harvested, filtered (0.45 μm) and

422 ultracentrifuged through a 20% (w/v) sucrose cushion. Virus pellets were then resuspended in

423 sterile filtered PBS 0.1% BSA, aliquoted and stored at -80°C. All replication competent

424 virions were handled in a BSL-3 containment laboratory.

425

426 **Lentiviral pseudotyping.** To generate lentiviral stocks, sub-confluent 293T cultures (15 cm²

427 dishes) were transfected with PEI as described above. Briefly, 22.5 μg of pWXPL-GFP

428 lentiviral backbone were co-transfected alongside 2.3 μg of pAdvantage, 15 μg packaging

429 vector Pax 2 and 8 μg of envelope glycoprotein encoding plasmids (VSVg, pcDNA Con1,

430 pcDNA JFH1). Lentiviral vectors carrying Vpx_{mac239} were produced in 293 T cells by co-

431 transfection of pWPI, pcDNA.Vpxmac239, pΔR8.9 NSDP, and VSV-G at a molar ratio of

432 4:1:3:1 as previously described (Pierini *et al.*, 2021). Cell culture supernatants were harvested

433 and filtered 3 days post transfection, and further concentrated through a 20% (w/v) sucrose

434 cushion ultracentrifugation. Aliquots were stored at -80°C. Virus titers were determined by

435 SG-PERT analysis (see below).

436

437   **Plasmids.** The proviral plasmids pNL4.3 WT and Δnef have been previously described

438   (Fackler *et al*, 2006). The pNL4.3-R5 WT & Δnef, containing 7 point mutations in the NL4.3

439   Env were previously described (Bozek *et al*, 2013; Pierini *et al.*, 2021). The pNL4.3 Δenv,

440   and HIV-2 Rod9-GFP proviruses were previously described (Baldauf *et al*, 2012), provirus

441   encoding the CCR5 tropic ADA provirus were via the NIH AIDS reagent program (ARP-

442   416)(Gendelman *et al*, 1988). All Transmitted/Founder strains were obtained via the NIH

443   AIDS reagent program (pCR-XL-TOPO CH077 (ARP-11742)(Ochsenbauer *et al*, 2012),

444   pCR-XL-TOPO CH058.c (ARP-11856)(Ochsenbauer *et al.*, 2012), pCR-XL-TOPO_HIV-1

445   M subtype C CH198 (Parrish *et al*, 2013). And chronic strains (pBR322 HIV-1 M subtype B

446   STCO (Mlcochova et al, 2015), pBR322 HIV-1 M subtype B RHGA(ARP-

447   12421)(Mlcochova *et al*, 2015), pUC57_HIV-1 M subtype C CH167(ARP-13544),

448   pUC57rev_HIV-1 M subtype C CH293(ARP-13539)(Parrish *et al.*, 2013). The following

449   expression plasmids were used: pMM311 (Vpr-BlaM) (Cavrois *et al.*, 2002), the

450   pmRuby2.Vpr vector was previously described (McDonald *et al*, 2002) and kindly provided

451   by Dr. Tom Hope. The pcDNA3.1 Vpx SIVmac239-Myc and the pΔ R8.9 packaging vector

452   harboring a Vpx binding motif were previously described (Baldauf *et al.*, 2012).

453

454   **Reagents.** The following antibodies were used: Zombie Violet dye (Biolegend), anti-p24 KC-

455   57 antibody (Beckman Coulter), 2G12 anti-gp120 antibody (NIH HIV Reagent program:

456   ARP-1476). The following dyes were used: Concanavalin A-488 (Sigma Aldrich) was used a

457   concentration of 50 µ/ml to stain TZM-bl cell membrane for 10 min at RT in the dark, Alexa

458   Fluor 488 NHS Ester (Invitrogen) was used to fluorescently label loose collagen gels as

459   described below, Fluoromount DAPI (Thermo Sci) was used to mount coverslips and stain

460   cell nuclei, the CCF2-AM dye (Thermo Scientific K1023) was used to perform HIV-1 entry

461   assays The following reagents were used PEI (Sigma Aldrich, Servapore dialysis membranes

462   (3.5 kDa MWCO, SERVA).

463

464 **Virus titer determination.** One step Syber Green based Product Enhanced Reverse

465 Transcriptase assay (SG-PERT) was used to assess HIV-1 virus titers as described previously

466 (Vermeire et al 2012). Briefly, concentrated virus stocks were first diluted in PBS, or culture

467 supernatants were directly lysed in 2x lysis buffer (50 mM KCL, 100 mM Tris-HCl pH 7.4,

468 40% glycerol, 0.25% Triton X-100) supplemented with 40 mU/µl Rnase inhibitor for 10

469 minutes at room temperature. Lysed samples were then exported from BSL-3 and further

470 diluted 1:10 in dilution buffer (5 mM $(NH_4)_2SO_4$, 20 mM KCL, 20 mM Tris-HCl pH 8). In

471 parallel, 10 µl per well of a dilution series of a virus standard (pCHIV, $8{,}09 \times 10^8$ pURT/µl)

472 were also lysed for 10 min. All lysed samples were then incubated with 10 µl of 2x reaction

473 buffer (1xdilution buffer, 10 mM $MgCl_2$. 2x BSA, 400 µM each dATP, dTTP, dCTP, dGTP,

474 1pmol of each RT forward and reverse primers, 8 ng MS2 RNA, SYBR Green 1:10000)

475 supplemented with 0.5U of GoTaq HotStart Polymerase. RT-PCR reactions were carried out

476 and read in a real-time PCR detector (CFX 96, Biorad) using the following program: (1) 42

477 °C for .20 min, (2) 95°C for 2 min, (3) 95°C for 5s, (4) 60°C for 5 s, (5) 72°C for 15 s, 80°C

478 for 7 s, repeat steps 3 to 6 for 40 cycles with a melting curve read out as a final step. Sequence

479 of the used primers are as follows: fwd RT primer (TCCTGCTCAACTTCCTGTCGAG) and

480 rev RT primer (CACAGGTCAAACCTCCTAGGAATG.)

481

482 **Virus infectivity determination.** To assess the infectivity of virus stocks, TZM-bl reporter

483 cells were infected as previously described (Wei *et al*, 2002). In brief, TZM-bl cells stably

484 expressing HIV-1 entry receptors and containing luciferase and β-galactosidase genes under

485 the control of the HIV-1 LTR promoter were infected using dilution series of concentrated

486 virus. 72h post-infection, cells were fixed in 3% PFA, and incubated with a substrate solution

487 (β-Gal supplemented with 200 µg/ml X-Gal) for 3h at 37°C. Blue cells were counted to

488 determine infectious virus titers in the form of Blue Cell Units (BCUs). For virus containing

21

489   cell culture supernatants, TZM-bl cells were infected in triplicates, and were lysed 3 days

490   post-infection using 1x lysis buffer (Promega) for 10 min. Lysates were then incubated with

491   Luciferase substrate (Promega), and luciferase activity was measured for 5s at a Tecan

492   Infinity luminometer.

493   For saturation experiments, 10^5, 10^6, or 10^7 BCUs were used for seeding or embedding in

494   collagen matrices of equivalent volumes. The culture supernatants were then processed by

495   SG-PERT. TZM-bl cells were infected using equivalent amounts of RT units for all

496   conditions. Virus infectivity after seeding or embedding at different concentrations was then

497   determined by measuring the average luciferase activity from cell lysates 3 days post

498   infection. To assess the relative infectivity of viruses after seeding or embedding, the

499   infectivity and RT activity of virus containing supernatants were assessed as described above.

500   The relative infectivity of the respective supernatants was calculated as the average luciferase

501   activity divided by the average amount of RT units measured from the culture supernatant.

502

503   **Virus embedding in 3D matrices.** Type I collagen matrices of different densities were

504   polymerized as previously described (Imle *et al.*, 2019). In brief, dense collagen gels (3

505   mg/ml) were generated by mixing 10X MEM medium with 7.5% $NaHCO_3$ (both Gibco) and

506   highly concentrated rat tail collagen I (Corning) at a 1:1:8 ratio on ice. Concentrated virus was

507   then added to the neutralized and chilled collagen solution at a 1:1 ratio. 100 µl of virus

508   containing collagen solutions were then distributed in each well in a 96 well-plate and

509   allowed to polymerize within 15 minutes at 37°C. Loose collagen gels (1.7 mg/ml) were

510   generated by mixing 10X MEM medium with 7.5% $NaHCO_3$ (both Gibco) and bovine skin

511   collagen I (PureCol, Advanced Biomatrix) at a 1:1:8 ratio on ice. Concentrated virus was then

512   added to the neutralized and chilled collagen solution at a 1:1 ratio and, and the mixture was

513   allowed to pre-polymerize for 10 min at 37°C. 100 µl per well were then transferred to a 96-

514   well plate. Gels were allowed to polymerize within 45 minutes at 37°C.

515   Human lyophilized placental type III collagen (Advance Biomatrix) was reconstituted using a

516   chilled 2 mM CH_3COOH solution on ice to reach 6 mg/ml. Type III collagen matrices (3

517   mg/ml) were generated by mixing 10X MEM with 7.5% $NaHCO_3$ (both Gibco) with the

518   reconstituted type III collagen solution at a 1:1:8 ratio on ice. Concentrated virus was then

519   added to the neutralized and chilled collagen solution at a 1:1 ratio. Gels were allowed to

520   polymerize within 30 min at 37°C.

521   Similarly, Matrigel (Matrigel Growth Factor Reduced Basement Membrane, Corning) gels (5

522   mg/ml) were generated according to manufacturer protocol. In brief, concentrated Matrigel

523   aliquots (8.9 mg/ml) were thawed at 4°C overnight. Thawed Matrigel was then combined

524   with DMEM containing concentrated virus at a 3:2 ratio on ice. 100 µl of mixture was

525   transferred to a 96-well plate, gels were allowed to polymerize within 45 min at 37°C.

526   Agarose gels were prepared by preparing a 0.8% agarose solution in PBS. The dissolved

527   agarose solution was combined 1:1 with DMEM containing concentrated virus. 100 µl of the

528   mixture was transferred to a 96-well plate, gels were allowed to polymerize at 4°C within 15

529   minutes.

530   All polymerized gels were then overlaid with pre-warmed with 100 µl DMEM and incubated

531   at 37°C. Culture supernatants were harvested at the indicated time points and processed for

532   relative infectivity determination.

533

534   **Fluorescent collagen gels.** Fluorescently labelled loose collagen gels were generated as

535   described previously (Sixt & Lammermann, 2011). In brief, 5 mg of Alexa Fluor 488 NHS

536   Ester dye (Invitrogen) was dissolved in 0.5 ml DMSO. The dissolved dye was then combined

537   with PureCol bovine skin collagen (3 mg/ml) at a 1:100 ratio on ice and stirred overnight at

538   4°C. After labelling, the excess dye was removed by dialysis using a 3.5 kDa molecular

539   weight cut off Servapore tubing (Serva), placed in 1 L of acetic acid solution (0.02 N, pH 3.9)

540   and stirred for one week at 4°C. The resulting collagen solution was kept at 4°C until further

541   use. Fluorescently labelled collagen gels were polymerized as described above, by combining

542   labelled and unlabelled collagen solutions at a 1:10 ratio.

543

544   **Western blot.** For detection of gp120 on virions from supernatants of suspension and

545   collagen cultures, supernatants were concentrated by ultracentrifugation through a 20%

546   sucrose cushion (44000 rpm, 45 min) using an Optima LE-80k ultracentrifuge (Beckman

547   Coulter), and lysed in 2x SDS sample buffer (10% glycerol, 6% SDS, 130 mM Tris Hcl pH

548   6.8, 10% β-Mercaptoethanol) and boiled for 5 min. Protein samples and were resolved with

549   SDS-PAGE electrophoresis and blotted onto nitrocellulose membranes. Membranes were

550   blocked in 4% milk/TBST for 1 h and were incubated with primary antibodies overnight. We

551   used secondary antibodies conjugated to IRDye700/800 (1:20000, Rockland) for fluorescent

552   detection with Licor (Odyssey).

553

554   **Confocal reflection microscopy.** Collagen gels were imaged by confocal reflection

555   microscopy as previously described (Imle *et al.*, 2019; Wolf *et al*, 2009). Briefly, different

556   collagen gels were generated in 15 well angiogenesis μ-slides (Ibidi) as described above.

557   Point laser scanning confocal microscopy was then performed on a Leica SP8 microscope

558   using an HC PL APO CS2 63x/1.4 N.A. oil immersion objective. Images were acquired using

559   PMT detectors in reflection mode with a laser excitation at 567 nm, and a spectral detection

560   window set between 550 nm and 570 nm wavelengths. Fluorescently stained collagen

561   matrices were additionally imaged using a 488 nm laser.

562

563   **Widefield imaging.** To assess the presence of fluorescently labelled collagen at the surface of

564   NL4.3 Vpr-mRuby2 virions, viruses were embedded in stained or unstained loose collagen

565   matrices   as   described   above.   The   culture   supernatants   were   then   harvested   and

566   ultracentrifuged through a 20% (w/v) sucrose cushion. Virus pellets were resuspended in 3%

567 PFA for 1h30. The fixed virus particles were then seeded on 0.01% poly-L-lysine coated

568 coverslips for 30 min and mounted on microscopy slides with Fluoromount DAPI

569 (Invitrogen). Samples were then imaged using an epifluorescence microscope (Olympus IX81

570 S1F-3) under a 100X oil objective (PlanApo, N.a. 1.40). Quantification of double positive

571 Vpr-mRuby2 and Alexa Fluor 488 signals was performed using the Spot Detector plugin of

572 the Icy Imaging analysis software.

573

574 **Harvesting of collagen fibers for cryo-ET analysis.** To assess the morphology of single

575 collagen fibers by cryo ET, dense or loose collagen gels were prepared as previously in 1.5 ml

576 Eppendorf tubes. Polymerized gels were disrupted by sonication on a Sonorex super RK 102

577 H sonicator for 10 sec on ice. Disrupted individual fibers were resuspended in PBS, and

578 further processed for cyro-ET.

579

580 **Plunge freezing.** Collagen fibers and supernatant for plunge freezing were collected as

581 described above. Holey carbon grids (Cu 200 mesh, R2/1, Quantifoil®) were plasma-cleaned

582 for 10 s in a Gatan Solarus 950 (Gatan). Samples were mixed with 10x concentrated 10 nm

583 protein A gold (Aurion) prior plunge freezing. A total volume of 3 µl was used for plunge

584 freezing into liquid ethane using an automatic plunge freezer EM GP2 (Leica). The ethane

585 temperature was set to −183 °C and the chamber to 24 °C with 80% humidity. Grids were

586 blotted from the back with Whatman™ Type 1 paper for 3 s. Grids were clipped into

587 AutoGrids™ (Thermo Fisher Scientific).

588

589 **Cryo-electron tomography and tomogram reconstruction.** Cryo-electron tomography was

590 performed using a Krios cryo-TEM (Thermo Fisher Scientific) operated at 300 keV and

591 equipped with a post-column BioQuantum Gatan Imaging energy filter (Gatan) and K3 direct

592 electron detector (Gatan) with an energy slit set to 15 eV. As a first step, positions on the grid

593   were mapped at 8,700× (pixel spacing of 10.64 Å) using a defocus of approximately -65 μm

594   in SerialEM (Mastronarde, 2005) to localize collagen fibers or HIV particles. Tilt series were

595   acquired using a dose-symmetric tilting scheme (Hagen *et al*, 2017) with a nominal tilt range

596   of 60° to -60° with 3° increments with SerialEM. Tilt series were acquired at target focus −4

597   μm, with an electron dose per record of 3 e$^-$/Å^2 and a magnification of 33,000× (pixel spacing

598   of 2.671 Å). Beam-induced sample motion and drift were corrected using MotionCor2 (Zheng

599   *et al*, 2017). Tilt series were aligned using AreTomo (Zheng *et al*, 2022) and tomograms were

600   reconstructed using R-weighted back projection algorithm with dose-weighting filter and

601   SIRT-like filter 5 in IMOD (Kremer *et al*, 1996). Tomograms were used to measure diameter

602   of HIV particles in IMOD. For visualization, tilt series were aligned using protein A gold as

603   fiducials in IMOD. Tomograms in Fig. 2 were reconstructed using R-weighted back

604   projection algorithm with 3DCTF, dose-weighting filter and SIRT-like filter 10. In IMOD, 15

605   slices of the final tomogram were averaged and Fourier filtered. The diameter of HIV

606   particles was measured from the outer leaflet of the viral membrane in IMOD. The average

607   diameter of two measurements per particle was used in the graph.

608

609   **Infectivity enhancement experiments.** Culture supernatants from suspension seeded or

610   collagen embedded virions were incubated with previously described infectivity enhancers to

611   overcome ERVI. In brief, equivalent amounts of RT units of virus containing supernatants

612   were incubated with different Peptide Nanofibrils (PNFs). EF-C (15 μg/ml) (Yolamanova *et*

613   *al.*, 2013) or RM-8 (15 μg/ml) (Rauch-Wirth L *et al.*, 2023) were then incubated for 20 min at

614   37°C prior to infection of TZM-bl cells. Relative infectivity of the treated virions was

615   assessed as described previously.

616

617   **Binding assay.** To assess the binding capacity of collagen and suspensions treated virions,

618   NL4.3 Vpr mRuby2 virions were seeded or embedded as previously described. Culture

619   supernatants were harvested 16h later, and viral titers were quantified by SG-PERT.

620   Equivalent amounts of RT units were then used to infect TZM-bl cells seeded on glass

621   coverslips in 24-well plates 24h prior to infection. Infection was carried out for 2h at 4°C to

622   prevent virion internalization. The cells were then washed with PBS, and the plasma

623   membrane was stained with Concanavalin A Alexa Fluor-488 (Invitrogen) according to

624   manufacturer protocol. The samples were then fixed using 3% PFA for 1h30, and mounted on

625   microscopy slides using Fluoromount-DAPI (Invitrogen). Spinning disk confocal microscopy

626   was performed on a PerkinElmer UltraVIEW VoX microscope equipped with Yokogawa

627   CSU-X1 spinning disk head and Nikon TiE microscope body. An Apo TIRF 60x/1.49 N.A.

628   oil immersion objective and a Hamamatsu C9100-23B EM-CCD camera were used. Images

629   were acquired using solid state lasers with excitation at 405nm, 488nm and 561nm with

630   matching emission filters. Z-stacks were acquired with a z-spacing of 0.5 µM steps. To assess

631   levels of virus binding between conditions, Z-stacks were 3D reconstructed using the Imaris

632   software (Oxford instruments). Cell membranes and virions were segmented as individual

633   surfaces, and statistic values (surface volumes, relative distance of surfaces) were exported by

634   the software.

635

636   **Vpr-BlaM entry Assay.** TZM-bl reporter cells were infected at MOI 0.1 using HIV-1

637   pNL4.3 viruses containing Vpr-BlaM, seeded in suspension or embedded in rat tail or bovine

638   collagen for 16 hours. Concentrated virus that was not seeded in medium prior to infection

639   was used as positive control, virus particles lacking Env were used as negative control. Fusion

640   of HIV-1 particles was allowed to proceed for 4 h at 37°C. Cells were then washed twice in

641   PBS and stained with 2mM CCF2-AM dye (Invitrogen) supplemented with 2.5 mM

642   Probenecid in Fluorobrite DMEM 2% FCS for 6 h at 11°C to prevent particle fusion during

643   the staining process according to manufacturer instructions. Where indicated, T20 was added

27

644 to block fusion. Cells were then trypsinized fixed in 3% PFA in PBS at 4°C overnight and

645 analyzed by FACS.

646

647 **Primary CD4+ T cell infection.** Activated primary CD4+ T cells were infected in 96-well

648 plated in triplicate with suspension and collagen culture supernatants containing NL4.3 R5 as

649 previously described (Imle *et al.*, 2019). Briefly, equivalent RT units were used between the

650 different conditions, as quantified by SG-PERT. The cells were spin-infected at 2000 rpm for

651 1h30 in presence or absence of 3 µg/ml reverse transcriptase inhibitor Efavirenz (EFZ), then

652 cultured at 37°C for 3 days. The samples were then stained with a fixable Zombie Violet dye

653 (Biolegend), fixed in 3% PFA for 1h30, then stained with an anti-p24 KC-57 FITC antibody

654 (Beckman Coulter) according to manufacturer protocol. Samples were then measured by flow

655 cytometry.

656

657 **Primary MDM infection.** Differentiated macrophages were spin transduced at 37°C in a pre-

658 heated centrifuge with lentiviral vectors containing Vpx_{mac239} for 1h at 300 rpm. Within 16h

659 post-transduction, cells were infected in triplicates with equivalent amounts of RT units as

660 measured by SG-PERT from suspension and collagen culture supernatants in a 96-well plate

661 format, in presence or absence of EFZ. MDMs were also treated with 50 ng/ml LPS as a

662 positive control. Infected MDM culture supernatants were harvested 3 days post-infection and

663 further processed for cytokine analysis. 5 days post-infection, cells were harvested by

664 trypsinization, and stained with a fixable Zombie Violet dye (Biolegend), fixed in 3% PFA for

665 1h30, then stained with an anti-p24 KC-57 FITC antibody (Beckman Coulter) according to

666 manufacturer protocol. Infection rates were then determined by flow cytometry.

667

668 **Modelling.** The mathematical model that we used previously to estimate the contribution of

669 cell-free and cell-to-cell transmission given different environmental conditions has been

670   described in detail within (Imle *et al.*, 2019). In brief, the model describes the turnover and

671   dynamics of (un-)infected CD4+ T cells, CD8+ T cells and the viral load within the different

672   culture systems by ordinary differential equations. The complete set of mathematical

673   equations and detailed description, as well as pre-defined parameter values used within the

674   analyses, are given within (Imle *et al.*, 2019). In the original publication, the model was fitted

675   simultaneously to the data of a co-transfer experiment of infected and uninfected CD4+ T

676   cells into 2D suspension, and 3D loose and dense collagen environments, with environmental

677   restriction reducing the infectivity of cell-free virions within collagen, i.e., the transmission

678   parameter β_f, to only 14% of the effectivity considered within suspension, i.e., $\beta_{f,loose} =$

679   $\beta_{f,dense} = \eta\beta_{f,sus}$ with $\eta = 0.14$. Here, we re-performed the analysis done within (Imle *et*

680   *al.*, 2019) by varying η between 0 and 1 within steps of 0.1, and also considering $\eta = 0.275$

681   as experimentally determined for primary target cells. Fitting was performed as described

682   within (Imle *et al.*, 2019) using the *optim*-function within the *R*-language of statistical

683   computing. Posterior distributions of parameter estimates were obtained by performing

684   ensemble fits for each value of η based on different starting values. Subsequent filtering steps

685   of fits ensured convergence of parameter estimates by excluding unreasonable dynamics of

686   CD4+ T cell counts and viral loads, with posterior distributions based on ~110-145 successful

687   fits for each value of η (see EV 4 A&B)).

688

689   **Flow cytometry.** Samples were measured by flow cytometry in BD FACS Celesta with BD

690   FACS Diva Software. Compensation controls were added for each experiment. Gating was

691   performed using FlowJo software 10.4.2 and data were processed in GraphPad Prism 8.4.3

692   software.

693

694   **TLR inhibitor treatments.** To determine the sensing pathway involved in collagen mediated

695   sensitization of virus particles for innate immune recognition, MDMs were pre-treated with

29

696 the different inhibitors prior to infection. 5 µM of cGAS inhibitor (G140, Invivogen), 8 µM of

697 TLR 1/2 inhibitor (Cu-CPT22, Selleckchem), 49 µM of TLR 4/6 inhibitor (GIT27, Tocris) or

698 10 µM of TLR 8 inhibitor (Cu-CPT9a, Invivogen) were incubated with MDMs 3h prior to

699 infection. The Myd-88 inhibitor (Pepinh-MYD, Invivogen) was used at 20 µM and incubated

700 with MDMs 4h prior to infection. Finally, MDMs were also pre-treated for 1h with a

701 TLR3/dsRNA complex inhibitor (Merck Millipore) 5 µM final concentration. MDMs were

702 also treated with 100 µM of T20 HIV-1 fusion inhibitor (Roche) or 3 µg/ml EFZ. The

703 different inhibitors were supplemented again during virus inoculation. The cells were then

704 cultured for 3 days at 37°C, and supernatants were harvested for cytokine analysis.

705

706 **Cytokine quantification.** The amounts of cytokines and chemokines present in cell culture

707 supernatants were determined by Eve Technologies Corporation using the Discovery Assay®:

708 Human Cytokine Array/Chemokine Array 48-Plex. Results are expressed in pg/ml of

709 cytokines/chemokines according to the company protein standard. Cell-free supernatants were

710 also analyzed for levels of Il-6, Il-8 and TNF-α by enzyme-linked immunosorbent assay

711 (ELISA; BD Biosciences) according to manufacturer's instructions.

712

713 **Statistical analysis.** Statistical analysis of datasets was carried out using Prism version 8.4.3

714 (GraphPad). Statistical significance was calculated using paired or unpaired one-way

715 ANOVA tests, as well as Wilcoxon matched paired test. Correction for multiple comparisons

716 are indicated in figure legends. n.s., not significant; *, $p < 0.05$; **, $p < 0.01$, ***$p < 0,005$.

717

718 **Acknowledgments**

722   Christine Selhuber Unkel and Ada Cavalcanti-Adam for advice and discussion and to Volker

723   Lohmann, Frank Kirchhoff and Tom Hope for sharing reagents.

724

725   **Author Contributions**

726   Conceptualization, O.T.F.; Methodology, S.S.A., F.G., Investigation, S.S.A., L.Z., A.I., N.T.,

727   K.W.; Data analysis, S.S.A., L.Z.; Bioinformatic analysis, K.W., F.G.; Writing – Original

728   Draft, O.T.F., S.S.A., L.Z. and F.G.; Writing – Review & Editing, O.T.F, S.S.A., F.G., P.C.;

729   Funding Acquisition, O.T.F.; Resources, L.R., J.M.; Supervision, O.T.F, P.C., F.G.

730

731   **Declaration of Interests**

732   The authors declare no competing interests.

733

References

Ahmed SS, Bundgaard N, Graw F, Fackler OT (2020) Environmental Restrictions: A New Concept Governing HIV-1 Spread Emerging from Integrated Experimental-Computational Analysis of Tissue-Like 3D Cultures. *Cells* 9

Anguiano M, Morales X, Castilla C, Pena AR, Ederra C, Martínez M, Ariz M, Esparza M, Amaveda H, Mora M *et al* (2020) The use of mixed collagen-Matrigel matrices of increasing complexity recapitulates the biphasic role of cell adhesion in cancer cell migration: ECM sensing, remodeling and forces at the leading edge of cancer invasion. *PLoS One* 15: e0220019

Bahraoui E, Serrero M, Planès R (2020) HIV-1 Tat - TLR4/MD2 interaction drives the expression of IDO-1 in monocytes derived dendritic cells through NF-κB dependent pathway. *Sci Rep* 10: 8177

Baldauf HM, Pan X, Erikson E, Schmidt S, Daddacha W, Burggraf M, Schenkova K, Ambiel I, Wabnitz G, Gramberg T *et al* (2012) SAMHD1 restricts HIV-1 infection in resting CD4(+) T cells. *Nat Med* 18: 1682-1687

Boesze-Battaglia K, Clayton ST, Schimmel RJ (1996) Cholesterol redistribution within human platelet plasma membrane: evidence for a stimulus-dependent event. *Biochemistry* 35: 6664-6673

Bozek K, Lengauer T, Sierra S, Kaiser R, Domingues FS (2013) Analysis of physicochemical and structural properties determining HIV-1 coreceptor usage. *PLoS Comput Biol* 9: e1002977

Braun E, Hotter D, Koepke L, Zech F, Groß R, Sparrer KMJ, Müller JA, Pfaller CK, Heusinger E, Wombacher R *et al* (2019) Guanylate-Binding Proteins 2 and 5 Exert Broad Antiviral Activity by Inhibiting Furin-Mediated Processing of Viral Envelope Proteins. *Cell Rep* 27: 2092-2104.e2010

Brügger B, Glass B, Haberkant P, Leibrecht I, Wieland FT, Kräusslich HG (2006) The HIV lipidome: a raft with an unusual composition. *Proc Natl Acad Sci U S A* 103: 2641-2646

Cavrois M, De Noronha C, Greene WC (2002) A sensitive and specific enzyme-based assay detecting HIV-1 virion fusion in primary T lymphocytes. *Nat Biotechnol* 20: 1151-1154

Chertova E, Bess JW, Jr., Crise BJ, Sowder IR, Schaden TM, Hilburn JM, Hoxie JA, Benveniste RE, Lifson JD, Henderson LE *et al* (2002) Envelope glycoprotein incorporation, not shedding of surface envelope glycoprotein (gp120/SU), Is the primary determinant of SU content of purified human immunodeficiency virus type 1 and simian immunodeficiency virus. *J Virol* 76: 5315-5325

Chojnacki J, Staudt T, Glass B, Bingen P, Engelhardt J, Anders M, Schneider J, Müller B, Hell SW, Kräusslich HG (2012) Maturation-dependent HIV-1 surface protein redistribution revealed by fluorescence nanoscopy. *Science* 338: 524-528

Choudhry V, Zhang MY, Harris I, Sidorov IA, Vu B, Dimitrov AS, Fouts T, Dimitrov DS (2006) Increased efficacy of HIV-1 neutralization by antibodies at low CCR5 surface concentration. *Biochem Biophys Res Commun* 348: 1107-1115

Chow JC, Young DW, Golenbock DT, Christ WJ, Gusovsky F (1999) Toll-like receptor-4 mediates lipopolysaccharide-induced signal transduction. *J Biol Chem* 274: 10689-10692

Day JR, Münk C, Guatelli JC (2004) The membrane-proximal tyrosine-based sorting signal of human immunodeficiency virus type 1 gp41 is required for optimal viral infectivity. *J Virol* 78: 1069-1079

Del Cornò M, Cappon A, Donninelli G, Varano B, Marra F, Gessani S (2016) HIV-1 gp120 signaling through TLR4 modulates innate immune activation in human macrophages and the biology of hepatic stellate cells. *J Leukoc Biol* 100: 599-606

Dimitrov DS, Willey RL, Sato H, Chang LJ, Blumenthal R, Martin MA (1993) Quantitation of human immunodeficiency virus type 1 infection kinetics. *J Virol* 67: 2182-2190

Estes JD (2013) Pathobiology of HIV/SIV-associated changes in secondary lymphoid tissues. *Immunol Rev* 254: 65-77

Fackler OT, Moris A, Tibroni N, Giese SI, Glass B, Schwartz O, Kräusslich HG (2006) Functional characterization of HIV-1 Nef mutants in the context of viral infection. *Virology* 351: 322-339

Fackler OT, Peterlin BM (2000) Endocytic entry of HIV-1. *Curr Biol* 10: 1005-1008

Foli A, Saville MW, Baseler MW, Yarchoan R (1995) Effects of the Th1 and Th2 stimulatory cytokines interleukin-12 and interleukin-4 on human immunodeficiency virus replication. *Blood* 85: 2114-2123

Gallucci L, Abele T, Fronza R, Stolp B, Laketa V, Sid Ahmed S, Flemming A, Müller B, Göpfrich K, Fackler OT (2023) Tissue-like environments shape functional interactions of HIV-1 with immature dendritic cells. *EMBO Rep* 24: e56818

Gendelman HE, Orenstein JM, Martin MA, Ferrua C, Mitra R, Phipps T, Wahl LA, Lane HC, Fauci AS, Burke DS *et al* (1988) Efficient isolation and propagation of human immunodeficiency virus on recombinant colony-stimulating factor 1-treated monocytes. *J Exp Med* 167: 1428-1441

Gringhuis SI, van der Vlist M, van den Berg LM, den Dunnen J, Litjens M, Geijtenbeek TB (2010) HIV-1 exploits innate signaling by TLR8 and DC-SIGN for productive infection of dendritic cells. *Nat Immunol* 11: 419-426

Hagen WJH, Wan W, Briggs JAG (2017) Implementation of a cryo-electron tomography tilt-scheme optimized for high resolution subtomogram averaging. *J Struct Biol* 197: 191-198

Heil F, Hemmi H, Hochrein H, Ampenberger F, Kirschning C, Akira S, Lipford G, Wagner H, Bauer S (2004) Species-specific recognition of single-stranded RNA via toll-like receptor 7 and 8. *Science* 303: 1526-1529

Hoshino S, Konishi M, Mori M, Shimura M, Nishitani C, Kuroki Y, Koyanagi Y, Kano S, Itabe H, Ishizaka Y (2010) HIV-1 Vpr induces TLR4/MyD88-mediated IL-6 production and reactivates viral production from latency. *J Leukoc Biol* 87: 1133-1143

Hubner W, McNerney GP, Chen P, Dale BM, Gordon RE, Chuang FY, Li XD, Asmuth DM, Huser T, Chen BK (2009) Quantitative 3D video microscopy of HIV transfer across T cell virological synapses. *Science* 323: 1743-1747

Imle A, Kumberger P, Schnellbacher ND, Fehr J, Carrillo-Bustamante P, Ales J, Schmidt P, Ritter C, Godinez WJ, Muller B *et al* (2019) Experimental and computational analyses reveal that environmental restrictions shape HIV-1 spread in 3D cultures. *Nat Commun* 10: 2144

Iwami S, Takeuchi JS, Nakaoka S, Mammano F, Clavel F, Inaba H, Kobayashi T, Misawa N, Aihara K, Koyanagi Y *et al* (2015) Cell-to-cell infection by HIV contributes over half of virus infection. *Elife* 4

Jolly C, Kashefi K, Hollinshead M, Sattentau QJ (2004) HIV-1 cell to cell transfer across an Env-induced, actin-dependent synapse. *J Exp Med* 199: 283-293

Jones MG, Andriotis OG, Roberts JJ, Lunn K, Tear VJ, Cao L, Ask K, Smart DE, Bonfanti A, Johnson P *et al* (2018) Nanoscale dysregulation of collagen structure-function disrupts mechano-homeostasis and mediates pulmonary fibrosis. *Elife* 7

Kolodkin-Gal D, Hulot SL, Korioth-Schmitz B, Gombos RB, Zheng Y, Owuor J, Lifton MA, Ayeni C, Najarian RM, Yeh WW *et al* (2013) Efficiency of cell-free and cell-associated virus in mucosal transmission of human immunodeficiency virus type 1 and simian immunodeficiency virus. *J Virol* 87: 13589-13597

Krapp C, Hotter D, Gawanbacht A, McLaren PJ, Kluge SF, Stürzel CM, Mack K, Reith E, Engelhart S, Ciuffi A *et al* (2016) Guanylate Binding Protein (GBP) 5 Is an Interferon-Inducible Inhibitor of HIV-1 Infectivity. *Cell Host Microbe* 19: 504-514

Kremer JR, Mastronarde DN, McIntosh JR (1996) Computer visualization of three-dimensional image data using IMOD. *J Struct Biol* 116: 71-76

Li Y, Wang Z, Hou Y, Liu X, Hong J, Shi X, Huang X, Zhang T, Liao X, Zhang L (2023) Novel TLR7/8 agonists promote activation of HIV-1 latent reservoirs and human T and NK cells. *Front Microbiol* 14: 1033448

Liu Y, Fu Y, Wang Q, Li M, Zhou Z, Dabbagh D, Fu C, Zhang H, Li S, Zhang T *et al* (2019) Proteomic profiling of HIV-1 infection of human CD4(+) T cells identifies PSGL-1 as an HIV restriction factor. *Nat Microbiol* 4: 813-825

Lodermeyer V, Suhr K, Schrott N, Kolbe C, Stürzel CM, Krnavek D, Münch J, Dietz C, Waldmann T, Kirchhoff F *et al* (2013) 90K, an interferon-stimulated gene product, reduces the infectivity of HIV-1. *Retrovirology* 10: 111

Lopez P, Ajibola O, Pagliuzza A, Zayats R, Koh WH, Herschhorn A, Chomont N, Murooka TT (2022) T cell migration potentiates HIV infection by enhancing viral fusion and integration. *Cell Rep* 38: 110406

Maréchal V, Arenzana-Seisdedos F, Heard JM, Schwartz O (1999) Opposite effects of SDF-1 on human immunodeficiency virus type 1 replication. *J Virol* 73: 3608-3615

Maréchal V, Clavel F, Heard JM, Schwartz O (1998) Cytosolic Gag p24 as an index of productive entry of human immunodeficiency virus type 1. *J Virol* 72: 2208-2212

Maréchal V, Prevost MC, Petit C, Perret E, Heard JM, Schwartz O (2001) Human immunodeficiency virus type 1 entry into macrophages mediated by macropinocytosis. *J Virol* 75: 11166-11177

Mastronarde DN (2005) Automated electron microscope tomography using robust prediction of specimen movements. *J Struct Biol* 152: 36-51

McDonald D, Vodicka MA, Lucero G, Svitkina TM, Borisy GG, Emerman M, Hope TJ (2002) Visualization of the intracellular behavior of HIV in living cells. *J Cell Biol* 159: 441-452

Meås HZ, Haug M, Beckwith MS, Louet C, Ryan L, Hu Z, Landskron J, Nordbø SA, Taskén K, Yin H *et al* (2020) Sensing of HIV-1 by TLR8 activates human T cells and reverses latency. *Nat Commun* 11: 147

Medzhitov R, Preston-Hurlburt P, Kopp E, Stadlen A, Chen C, Ghosh S, Janeway CA, Jr. (1998) MyD88 is an adaptor protein in the hToll/IL-1 receptor family signaling pathways. *Mol Cell* 2: 253-258

Mlcochova P, Apolonia L, Kluge SF, Sridharan A, Kirchhoff F, Malim MH, Sauter D, Gupta RK (2015) Immune evasion activities of accessory proteins Vpu, Nef and Vif are conserved in acute and chronic HIV-1 infection. *Virology* 482: 72-78

Murooka TT, Deruaz M, Marangoni F, Vrbanac VD, Seung E, von Andrian UH, Tager AM, Luster AD, Mempel TR (2012) HIV-infected T cells are migratory vehicles for viral dissemination. *Nature* 490: 283-287

Neil SJ, Zang T, Bieniasz PD (2008) Tetherin inhibits retrovirus release and is antagonized by HIV-1 Vpu. *Nature* 451: 425-430

Nieto-Garai JA, Arboleya A, Otaegi S, Chojnacki J, Casas J, Fabriàs G, Contreras FX, Kräusslich HG, Lorizate M (2021) Cholesterol in the Viral Membrane is a Molecular Switch Governing HIV-1 Env Clustering. *Adv Sci (Weinh)* 8: 2003468

Ochsenbauer C, Edmonds TG, Ding H, Keele BF, Decker J, Salazar MG, Salazar-Gonzalez JF, Shattock R, Haynes BF, Shaw GM *et al* (2012) Generation of transmitted/founder HIV-1 infectious molecular clones and characterization of their replication capacity in CD4 T lymphocytes and monocyte-derived macrophages. *J Virol* 86: 2715-2728

Oh DY, Taube S, Hamouda O, Kücherer C, Poggensee G, Jessen H, Eckert JK, Neumann K, Storek A, Pouliot M *et al* (2008) A functional toll-like receptor 8 variant is associated with HIV disease restriction. *J Infect Dis* 198: 701-709

Parrish NF, Gao F, Li H, Giorgi EE, Barbian HJ, Parrish EH, Zajic L, Iyer SS, Decker JM, Kumar A *et al* (2013) Phenotypic properties of transmitted founder HIV-1. *Proc Natl Acad Sci U S A* 110: 6626-6633

Phillips DM (1994) The role of cell-cell transmission in HIV-1 infection. *AIDS*

Pierini V, Gallucci L, Stürzel CM, Kirchhoff F, Fackler OT (2021) SERINC5 Can Enhance Proinflammatory Cytokine Production by Primary Human Myeloid Cells in Response to Challenge with HIV-1 Particles. *J Virol* 95

Poli G, Kinter AL, Fauci AS (1994) Interleukin 1 induces expression of the human immunodeficiency virus alone and in synergy with interleukin 6 in chronically infected U1 cells: inhibition of inductive effects by the interleukin 1 receptor antagonist. *Proc Natl Acad Sci U S A* 91: 108-112

Rasaiyaah J, Tan CP, Fletcher AJ, Price AJ, Blondeau C, Hilditch L, Jacques DA, Selwood DL, James LC, Noursadeghi M *et al* (2013) HIV-1 evades innate immune recognition through specific cofactor recruitment. *Nature* 503: 402-405

Rauch-Wirth L RA, Kaygisiz K WT, Zimmermann L,, Rodriguez-Alfonso AA SD, Wiese S SL, Weil T, Schmiedel D, Münch J (2023) Optimized peptide nanofibrils as efficient transduction enhancers for in vitro and ex vivo gene transfer. *Front Immunol*

Rosa A, Chande A, Ziglio S, De Sanctis V, Bertorelli R, Goh SL, McCauley SM, Nowosielska A, Antonarakis SE, Luban J *et al* (2015) HIV-1 Nef promotes infection by excluding SERINC5 from virion incorporation. *Nature* 526: 212-217

Sáez-Cirión A, Nir S, Lorizate M, Agirre A, Cruz A, Pérez-Gil J, Nieva JL (2002) Sphingomyelin and cholesterol promote HIV-1 gp41 pretransmembrane sequence surface aggregation and membrane restructuring. *J Biol Chem* 277: 21776-21785

Schaeffer E, Soros VB, Greene WC (2004) Compensatory link between fusion and endocytosis of human immunodeficiency virus type 1 in human CD4 T lymphocytes. *J Virol* 78: 1375-1383

Sewald X, Ladinsky MS, Uchil PD, Beloor J, Pi R, Herrmann C, Motamedi N, Murooka TT, Brehm MA, Greiner DL *et al* (2015) Retroviruses use CD169-mediated trans-infection of permissive lymphocytes to establish infection. *Science* 350: 563-567

Shoulders MD, Raines RT (2009) Collagen structure and stability. *Annu Rev Biochem* 78: 929-958

Sixt M, Lammermann T (2011) In vitro analysis of chemotactic leukocyte migration in 3D environments. *Methods Mol Biol* 769: 149-165

Sourisseau M, Sol-Foulon N, Porrot F, Blanchet F, Schwartz O (2007) Inefficient human immunodeficiency virus replication in mobile lymphocytes. *J Virol* 81: 1000-1012

Usami Y, Wu Y, Göttlinger HG (2015) SERINC3 and SERINC5 restrict HIV-1 infectivity and are counteracted by Nef. *Nature* 526: 218-223

Venkatesh S, Bieniasz PD (2013) Mechanism of HIV-1 virion entrapment by tetherin. *PLoS Pathog* 9: e1003483

Vyakarnam A, McKeating J, Meager A, Beverley PC (1990) Tumour necrosis factors (alpha, beta) induced by HIV-1 in peripheral blood mononuclear cells potentiate virus replication. *Aids* 4: 21-27

Watala C, Waczulikova I, Wieclawska B, Rozalski M, Gresner P, Gwozdzinski K, Mateasik A, Sikurova L (2002) Merocyanine 540 as a fluorescent probe of altered membrane phospholipid asymmetry in activated whole blood platelets. *Cytometry* 49: 119-133

Wei X, Decker JM, Liu H, Zhang Z, Arani RB, Kilby JM, Saag MS, Wu X, Shaw GM, Kappes JC (2002) Emergence of resistant human immunodeficiency virus type 1 in patients receiving fusion inhibitor (T-20) monotherapy. *Antimicrob Agents Chemother* 46: 1896-1905

Wolf K, Alexander S, Schacht V, Coussens LM, von Andrian UH, van Rheenen J, Deryugina E, Friedl P (2009) Collagen-based cell migration models in vitro and in vivo. *Semin Cell Dev Biol* 20: 931-941

Yi L, Fang J, Isik N, Chim J, Jin T (2006) HIV gp120-induced interaction between CD4 and CCR5 requires cholesterol-rich microenvironments revealed by live cell fluorescence resonance energy transfer imaging. *J Biol Chem* 281: 35446-35453

Yin X, Langer S, Zhang Z, Herbert KM, Yoh S, König R, Chanda SK (2020) Sensor Sensibility-HIV-1 and the Innate Immune Response. *Cells* 9

Yolamanova M, Meier C, Shaytan AK, Vas V, Bertoncini CW, Arnold F, Zirafi O, Usmani SM, Müller JA, Sauter D *et al* (2013) Peptide nanofibrils boost retroviral gene transfer and provide a rapid means for concentrating viruses. *Nat Nanotechnol* 8: 130-136

Zheng S, Wolff G, Greenan G, Chen Z, Faas FGA, Bárcena M, Koster AJ, Cheng Y, Agard DA (2022) AreTomo: An integrated software package for automated marker-free, motion-corrected cryo-electron tomographic alignment and reconstruction. *J Struct Biol X* 6: 100068

Zheng SQ, Palovcak E, Armache JP, Verba KA, Cheng Y, Agard DA (2017) MotionCor2: anisotropic correction of beam-induced motion for improved cryo-electron microscopy. *Nat Methods* 14: 331-332

Figure legends

Figure 1: ERVI is Rapidly Induced, Saturable, and conserved across viruses and different types of matrices. A. Experimental workflow. HIV-1 NL4.3 viruses were seeded in suspension or embedded in type I collagen matrices of different densities. Supernatants of the cultures were harvested at different time points; RT activity was measured by SG-PERT and TZM-bl reporter cells were infected with equivalent volumes of culture supernatant to determine virion relative infectivity. B. Relative infectivity of HIV-1 NL4.3 particles after seeding or embedding for 16h. Data is normalized to suspension seeded virions (grey dotted line) Significance was calculated by one-way ANOVA test after Dunnett multiple comparison correction. C. Kinetics of ERVI. Culture supernatants were harvested at 0, 4, 8 or 16h post seeding/embedding and relative infectivity of virions was determined as in B. D. Conservation of ERVI across HIV-1, HIV-2 and single round lentiviral pseudotypes. Lab adapted HIV-1 strains (NL4.3, NL4.3 ΔNef, NL4.3 R5, ADA) as well as primary isolates (Transmitted/Founder: CH077, CH058.c and CH0198; Chronic; RHGA, CH0167, CH0293), but also HIV-2 Rod9 GFP and VSVg pseudotyped NL4.3 ΔEnv virions were seeded in suspension or embedded in collagen cultures for 16h as described in Fig.1.A. The relative infectivity of the virions was then assessed by SG-PERT and TZM-bl infection as previously described. Data is normalized to suspension condition for each virus (grey dotted line). Significance was calculated by one-way ANOVA test after Dunnett's multiple comparison correction. E. HCV lentiviral pseudotypes are more resistant to ERVI than VSVg pseudotypes. Lentiviral particles were seeded/embedded and Huh 7.5 cells were transduced as described in C. Transduced cells were quantified by flow cytometry analysis of GFP expressing cells 5 days post transduction. Data is normalized to suspension condition for each virus (grey dotted line). Significance was calculated by one-way ANOVA test by matched two-way ANOVA after Tukey correction. F. Saturation of ERVI. Increasing concentrations of virus were seeded or embedded in the equivalent volume of matrix/medium for 16h.

37

1028   Supernatants were then processed to determine the HIV-1 relative infectivity as in B.

1029   Significance was calculated by matched two-way ANOVA test after Tukey correction. G.

1030   Experimental workflow. HIV-1 NL4.3 viruses were seeded in suspension or embedded in

1031   different types of 3D matrices: dense or loose type I collagen matrices, human type III

1032   collagen matrices, Matrigel or agarose gels. Supernatants of the cultures were harvested 16h

1033   post seeding/embedding; RT activity was measured by SG PERT and TZM-bl reporter cells

1034   were infected with equivalent amounts of RT units for 3 days. The cells were then lysed, and

1035   infectivity was measured by assessing luciferase activity from cell lysates. H. Collagen

1036   containing matrices, but not agarose are able to restrict HIV-1 infectivity. Relative infectivity

1037   of HIV-1 NL4.3 particles after seeding or embedding in different matrices for 16h. Data is

1038   normalized to respective suspension seeded virions (grey dotted line). Significance was

1039   calculated by one-way ANOVA test after Dunnett's multiple comparison correction. Results

1040   represent the mean ± SD of 3 independent experiments. Symbols indicate data from

1041   individual experiments. *P<0.05; **P<0.001; ***P<0.005; n.s. not significant.

1042

1043   **Figure 2: ERVI does not result from collagen deposition or structural damages of**

1044   **embedded virions.** A. Relative infectivity of Vpr-mRuby2 containing HIV-1 NL4.3 virions,

1045   seeded in suspension or embedded in unstained, or AlexaFluor-488 stained loose collagen

1046   matrices for 16h. Data is normalized to suspension condition (Grey dotted line). Significance

1047   was calculated by one-way ANOVA test after Dunnett's multiple comparison correction. B.

1048   Representative micrographs of virions used in A. White arrows indicate Vpr-mRuby2 and

1049   AlexaFluor-488 positive virions. C. Quantification of the frequency of double positive events

1050   shown in panel C. Significance was calculated by unpaired one-way ANOVA test after

1051   Tukey's multiple comparison correction. D. Averaged slices of a tomogram showing HIV-1

1052   NL4.3 virions after 16h of culture in suspension (left panel), dense collagen (middle panel), or

1053   loose collagen (right panel). Scale bar = 50 nm. E. Quantification of the diameter of virus

1054   particles treated as indicated in D. Violin plot shows individual data points with

1055   corresponding median, 25% and 75% quartiles. Significance was calculated by unpaired t-

1056   tests. F. Averaged slices of a tomogram showing disrupted dense (left panel) or loose (right

1057   panel) collagen fibres. Scale bar = 100 nm. G. Experimental workflow. HIV-1 NL4.3 virions

1058   were seeded in suspension or embedded in collagen matrices as previously described. 16h

1059   post seeding/embedding, virions were harvested and equivalent amounts of RT units were

1060   incubated with infectivity enhancing peptides for 10 minutes prior to infection of TZM-bl

1061   reporter cells. H. Relative infectivity of PNF treated virions. Results represent the mean ± SD

1062   of 3 independent experiments. Symbols indicate individual experiments. *P<0.05;

1063   ***P<0.005; n.s. not significant.

1064

1065   **Figure 3: Collagen matrices do not affect the ability of viral particles to bind to target**

1066   **cells but triggers aggregation at the surface of target cells.** A. Experimental workflow.

1067   HIV-1 NL4.3 Vpr-mRuby2 virions were seeded in suspension or embedded in dense or loose

1068   collagen matrices for 16h. Culture supernatants were then collected, and equivalent amounts

1069   of RT units were incubated with TZM-bl cells for 2h at 4°C. Additionally virus particles that

1070   were not seeded in suspension for 16h (control, untreated virus) were used. Cell membranes

1071   were then stained using Concanavalin-A AF-488, prior to microscopy processing. B. Relative

1072   infectivity of HIV-1 NL4.3 Vpr-mRuby2 virions after seeding/embedding for 16h.

1073   Significance was calculated by one-way ANOVA test after Dunnett's multiple comparison

1074   correction. C. Representative micrographs of cells incubated with HIV-1 NL4.3 Vpr-mRuby2

1075   virions, either from concentrated stock, or seeded/embedded for 16h. Yellow arrows indicate

1076   Vpr-mRuby2+ spots detected at the surface of the target cells. Scale bar= 15 μm. D.

1077   Quantification of the average binding frequency of HIV-1 NL4.3 Vpr-mRuby2 virions to

1078   target cells as shown in C. Significance was calculated by one-way ANOVA test after

1079   Tukey's multiple comparison correction.E. Quantification of the average volume of the Vpr-

1080 mRuby2 spots detected as shown in C. Significance was calculated by one-way ANOVA test

1081 after Tukey's multiple comparison correction. Results represent the mean ± SD from 3

1082 independent experiment. Symbols indicate individual experiments. *P<0.05, **P<0.001,

1083 ***P<0.005; n.s. not significant.

1084

1085 **Figure 4: Collagen matrices impair viral fusion with target cells.** A. Experimental

1086 workflow. HIV-1 NL4.3 VprBlaM virions were seeded in suspension or embedded in dense

1087 or loose collagen matrices for 16h. Culture supernatants were then collected, and equivalent

1088 amounts of RT units were incubated with TZM-bl cells for 4h at 37°C, in the presence or

1089 absence of the T20 fusion inhibitor. Additionally, virus particles that were not seeded in

1090 suspension for 16h (control, untreated virus) were used. Cells were then loaded with the

1091 CCF2-AM dye for 10h at 11°C and processed by flow cytometry. B. Relative infectivity of

1092 HIV-1 NL4.3 VprBlaM virions 16h post seeding/embedding. Significance was calculated by

1093 unpaired one-way ANOVA test after Dunnets's multiple comparison correction. C.

1094 Representative flow cytometry dot plots depicting the appearance of CCF2 cleavage product

1095 by B-lactamase 4h post-infection. Gates indicate cells in which virus entry occurred. D.

1096 Quantification of the percentage of CCF2-product positive cells measured by flow cytometry.

1097 Significance was calculated by one-way ANOVA test after Tukey's multiple comparison

1098 correction. E. Reduction of HIV-1 virus entry in TZM-bl target cells correlates with their

1099 reduced relative infectivity after ERVI. Correlation between Relative Infectivity was assessed

1100 by linear regression. Results represent the mean ± SD from 3 independent experiments.

1101 Symbols indicate individual experiments. *P<0.05; **P<0.001; **P<0.005, n.s.: not

1102 significant.

1103

1104 **Figure 5: ERVI does not affect infection of primary cells but sensitizes virus particles for**

1105 **innate immune recognition by MDMs.** A. Experimental workflow. HIV-1 NL4.3 R5 virions

1106 were seeded in suspension or embedded in dense or loose collagen matrices for 16h. Culture

1107 supernatants were then collected, and equivalent amounts of RT units were incubated with

1108 MDMs or activated CD4+ T cells, in the presence or absence of the reverse transcription

1109 inhibitor Efavirenz. CD4+ T cells were harvested 3 days post infection for p24 quantification

1110 by flow cytometry. Supernatants from MDMs were harvested 3 days post infection for

1111 cytokine analysis, and cells were harvested 5 days post infection for p24 quantification by

1112 flow cytometry. B. Relative infectivity of HIV-1 NL4.3 R5 virions 16h post

1113 seeding/embedding. Significance was calculated by unpaired one-way ANOVA test after

1114 Tukey's multiple comparison correction C. Quantification of the percentage of p24+ CD4+ T

1115 cells by flow cytometry. CD4+ T cells were activated using Dynabeads for 3 days prior to

1116 infection and treated as described in A. Data is displayed for 4 independent donors.

1117 Significance was calculated by matched two-way ANOVA test after Tukey's multiple

1118 comparison correction. D. Quantification of the percentage of p24+ MDMs by flow

1119 cytometry. Monocytes were differentiated to MDMs for 10 days and transduced with Vpx-

1120 VLPs 16h prior to infection. Cells were then treated as described in A. Graphs depict mean

1121 values ± SD for 6 donors. Significance was calculated by matched two-way ANOVA test

1122 after Tukey's multiple comparison correction. E. Estimated fraction of cells infected by cell-

1123 free transmission after 21 days for the three environmental conditions given different values

1124 for the reduced efficacy of virion infectivity by ERVI, η. The plots show the posterior

1125 distributions of estimates over ~110-140 fits per value of η with dots indicating the estimate

1126 of the best model fit (see also Materials & Methods). Results for measured values of $\eta = 0.14$

1127 (Imle et al. 2019) and $\eta = 0.275$ (here) are shown in light colours. Results represent the mean

1128 ± SD from 3independent experiments, or 4/5 5 independent donors. *P<0.05; **P<0.001; n.s.:

1129 not significant.

41

1130

1131 **Figure 6: ERVI sensitizes HIV-1 virions for TLR-8 and TLR-4 innate immune**

1132 **recognition.** A. Experimental workflow. Monocytes were differentiated into MDMs for 10

1133 days as described previously. MDMs were then challenged with HIV-1 NL4.3 R5 virus that

1134 was kept in suspension or collagen, in presence or absence of TLR inhibitors, Efavirenz or

1135 T20 for 3 days. Culture supernatants were then harvested and processed for IL-6 and IL-8

1136 ELISA. B. Cytokine profiling of the supernatants of infected MDMs. Supernatants of infected

1137 MDMs were harvested 3 days post infection and processed for cytokine analysis. Heatmaps

1138 indicate Log2 fold change of cytokines in infected conditions as compared to mock infected

1139 conditions for 2 donors. Cytokines that were induced by dense collagen cultured virions >5-

1140 fold as compared to suspension conditions for both donors are highlighted in red. C. IL-6

1141 concentration determined by ELISA analysis of infected MDM supernatants. MDMs were

1142 infected with HIV-1 NL4.3 R5 kept in suspension or dense collagen in presence or absence of

1143 antiviral drugs or PRR inhibitors as described in A. Supernatants were harvested 3 days post

1144 infection and processed by ELISA for IL-6 concentration determination. Data is normalized to

1145 mock infected condition. Significance was calculated by matched two-way ANOVA test after

1146 Tukey's multiple comparison correction. Results represent the mean ± SD from 3 independent

1147 donors. Symbols indicate individual donors. ∗P<0.05; **P<0.001; ***P<0.005; n.s.: not

1148 significant.

1149

1150 **Figure 7: Schematic model of reduction of cell-free virion infectivity and sensitization**

1151 **for innate immune recognition by ERVI.** Physical contact with collagen fibers reduces the

1152 ability of HIV-1 particles to fuse with target cells, resulting in the recognition of HIV-1 Env

1153 by TLR-4 or their uptake via an alternative pathway in which TLR-8-mediated sensing of the

1154 HIV-1 genome occurs. Triggering of TLR-4 and -8 results in increased production of

1155 proinflammatory cytokines. See text for details.

1156

1157 **Extended View 1: Determinants of virus sensitivity to ERVI and assessment of different**

1158 **matrices.** Collagen embedding does not lead to Env shedding. HIV-1 NL4.3 virions were

1159 seeded in suspension or dense collagen cultures for 24h. Viruses were then collected from

1160 culture supernatants and concentrated by ultracentrifugation, and analyzed by western blot

1161 using the Licor technology. The gp120/gp41 ratio was determined by incubation of

1162 membranes with a human anti-gp120 antibody (2G12) and subsequent secondary antibodies

1163 conjugated to IRDye700/800 for fluorescent detection with Licor. Membranes were also

1164 blotted using a rabbit anti-p24 antibody as loading control. One representative blot is shown.

1165 B. Quantification of the gp120:p24 ratio from Western blots as in A. Significance was

1166 calculated by Wilcoxon matched paired test. C. Lentiviral pseudotype transduce Huh 7.5 cells

1167 more efficiently than Tzm-bl cells. Lentiviral particles were pseudotyped with type I (HA,

1168 Ebola virus GP), type II (HCV strains Con1 & JFH1) or type III (VSVg) fusion glycoproteins.

1169 TZM-bl or Huh 7.5 cells were transduced with lentiviral vectors for 5 days, and the

1170 percentage of GFP+ cells was quantified by flow cytometry. Data from one experiment is

1171 shown. D. Culture of lentiviral pseudotypes has differential effects on their infectivity.

1172 Lentiviral pseudotypes as in C. were seeded in suspension, dense or loose collagen cultures

1173 for 16h. Huh 7.5 cells were then transduced with equivalent RT units for each virus for 5

1174 days. The percentage of GFP+ cells was then quantified by flow cytometry. Data from one

1175 experiment is shown. E. Representative confocal auto-reflection micrographs of different 3D

1176 matrices. Different matrices were polymerized (see methods section) in 15-well Ibidi slides

1177 and imaged by confocal microscopy to assess fiber morphology and density. Scale bar: 10

1178 μm. Data is representative of one or three independent experiments. Results represent the

1179 mean ± SD from 3 independent donors. Symbols indicate individual donors. n.s.: not

1180 significant.

1181

Extended View 2: Characterization of collagen fibers. A. Representative confocal micrographs of fluorescently stained loose collagen gels. Acid dissolved loose collagen was stained using AlexaFluor-488 NHS Ester dye (see Materials & methods section). Fluorescently stained collagen gels were obtained by mixing stained and unstained collagen at a 1:10 ratio. Samples were then imaged by confocal microscopy, illuminated using a 488 nm laser for fluorescence detection, and imaged by auto-reflection. Scale bar: 10 µm. B. Low magnification image of collagen fibers on EM grids. Scale bar: 1 µm.

Extended View 3: Establishment of a workflow for automated detection of surface bound HIV-1 particles. HIV-1 NL4.3 VprmRuby2 virions were seeded in suspension or collagen cultures for 16h. Supernatants were harvested, and equivalent amounts of RT units were used to infect TZM-bl cells for 2h at 4°C. After staining of plasma membrane using Concanavalin-A 488, cells were fixed and processed for spinning disk microscopy image acquisition. The resulting z-stacks were loaded in Imaris for 3D reconstruction (left panel: raw data). Virions were segmented using the 568 channel and the "surfaces" tool in Imaris, with appropriate intensity and background thresholds (middle panel: red surfaces indicate segmented virions). Next, cells were then segmented using the DAPI and 488 channels, respectively staining nuclei and cellular membranes, by using the "cells" segmentation tool in Imaris (right panel: colored surfaces indicate single segmented cells). After segmentation, quantification of bound virus was performed by the quantification of virus surfaces that were distant no more than 0.5 µm of the nearest segmented cell surface. Quantification of the volumes of segmented virions was also performed by Imaris.

Extended View 4: **Modelling the impact of ERVI on HIV-1 spread in collagen lymphocyte cultures.** A. Filtering process of individual model fits to ensure comparability of estimates for different reduced efficacies η, used within the mathematical model shown in

44

1208 (Imle et al. 2019). A sequence of different filtering steps is applied to the results of the

1209 ensemble fits given different starting conditions only considering fits with residual sum of

1210 squares (RSS) $<10^4$ (filter 1), disregarding fits with predictions of >6000 cells after 12.5 days

1211 or viral concentrations $> 10^{6.8}$ RT μl^{-1} after 21 days in the supernatant for loose collagen (filter

1212 2), disregarding fits with $>7.5\times10^4$ CD4 T cells after 5 days in suspension (filter 3), and

1213 excluding fits with >5000 CD4 T cells within the first 5 days or $>2\times10^4$ cells after 20 days for

1214 dense collagen. The procedure is repeated to ensure comparable number of estimates for each

1215 value of η after the filtering for the analysis. B. Number of fits per value of η considered

1216 within the analyses. C. Distribution of estimates for the individual parameters describing cell

1217 infection dynamics within suspension and 3D collagen environments. Results of the best fit

1218 for each value of η are indicated by the white dot. For the meaning of the individual

1219 parameters and specific model equations see Imle et al., 2019.

1220

1221 **Extended View 5: ERVI induces IL-8 production by MDMs via TLR-8 sensing.** A.

1222 Supernatants form infected MDMs were harvested 3 days post infection and processed by

1223 ELISA for IL-8 concentration determination. Significance was calculated by paired one-way

1224 ANOVA after Dunnett's multiple comparison correction. Results represent the mean $\pm$ SD for

1225 3 independent donors. Symbols indicate individual donors. p*<0.05.

1226
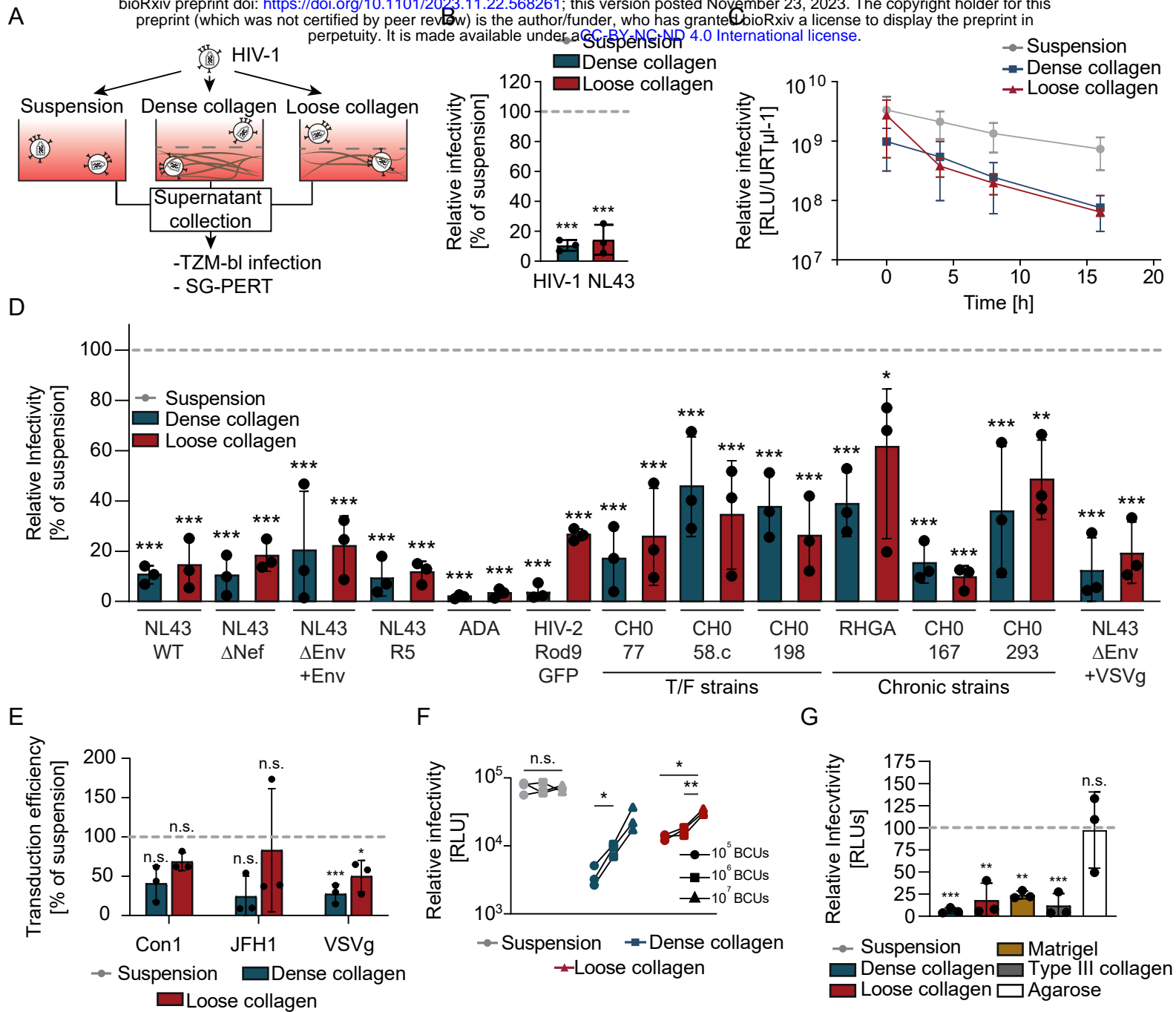
Fig. 1: Sid Ahmed et al, 2023
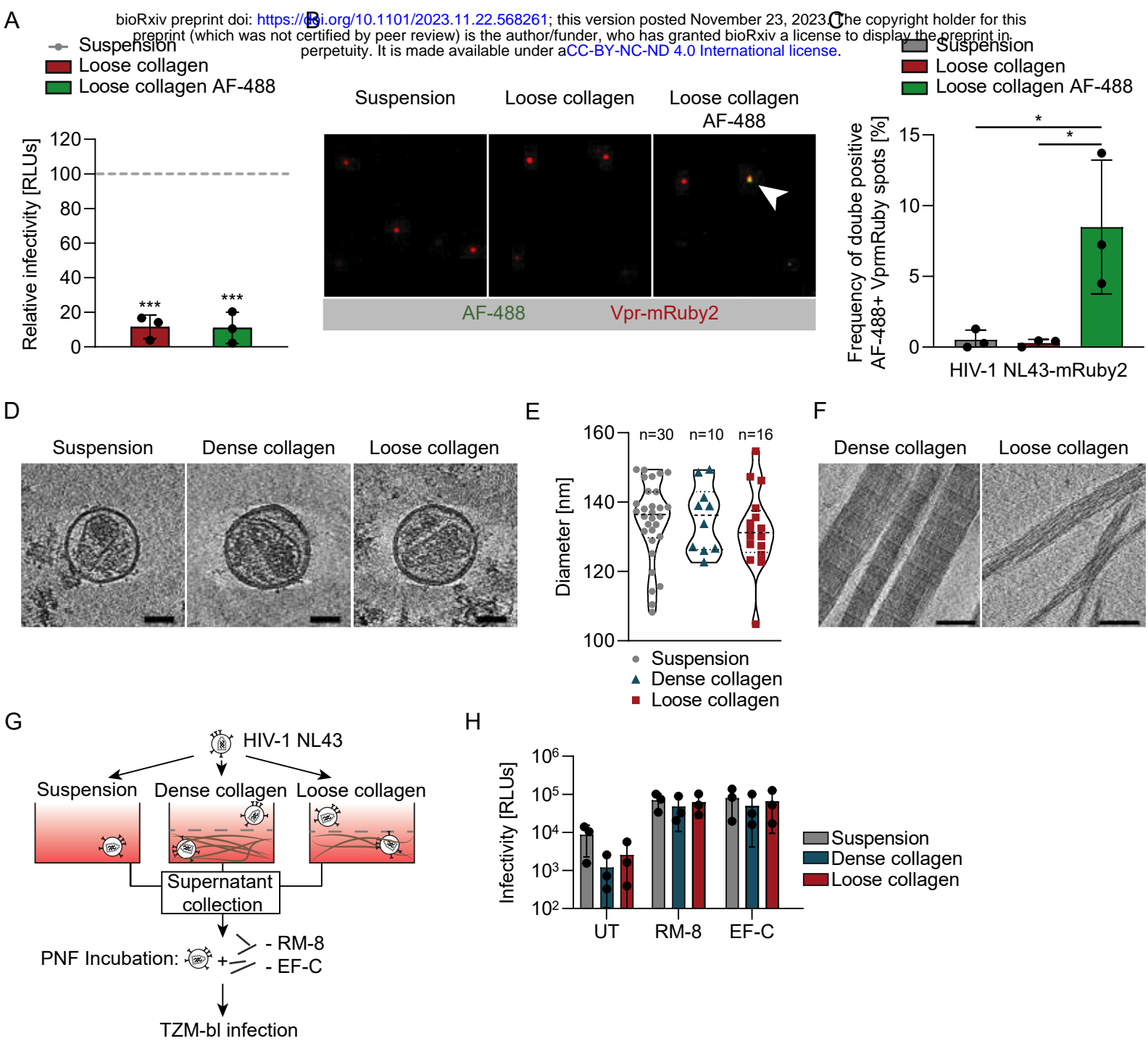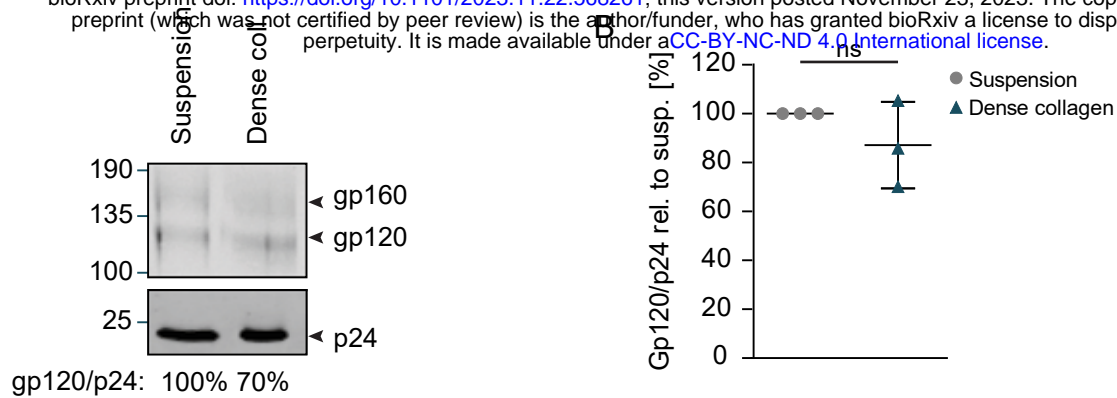
Fig. 2: Sid Ahmed et al, 2023
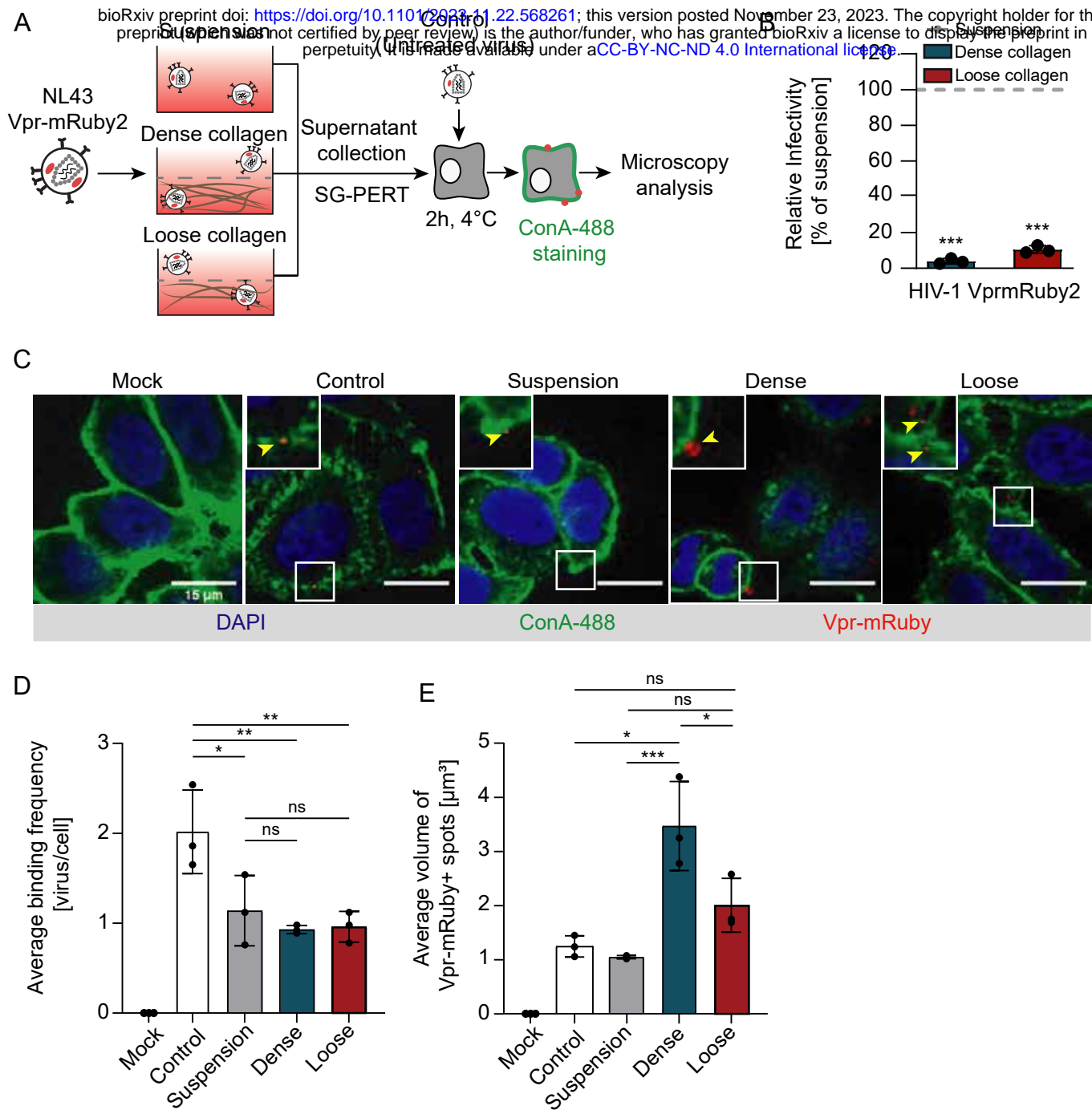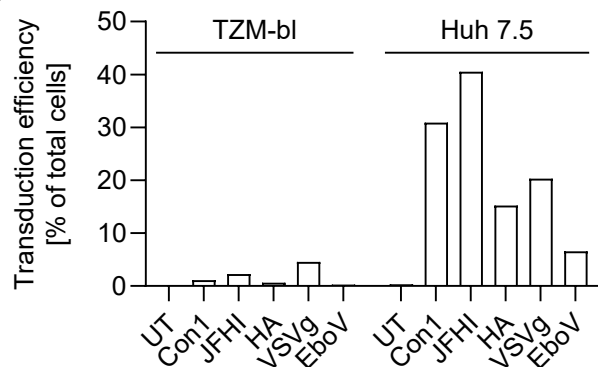
Fig. 3: Sid Ahmed et al, 2023
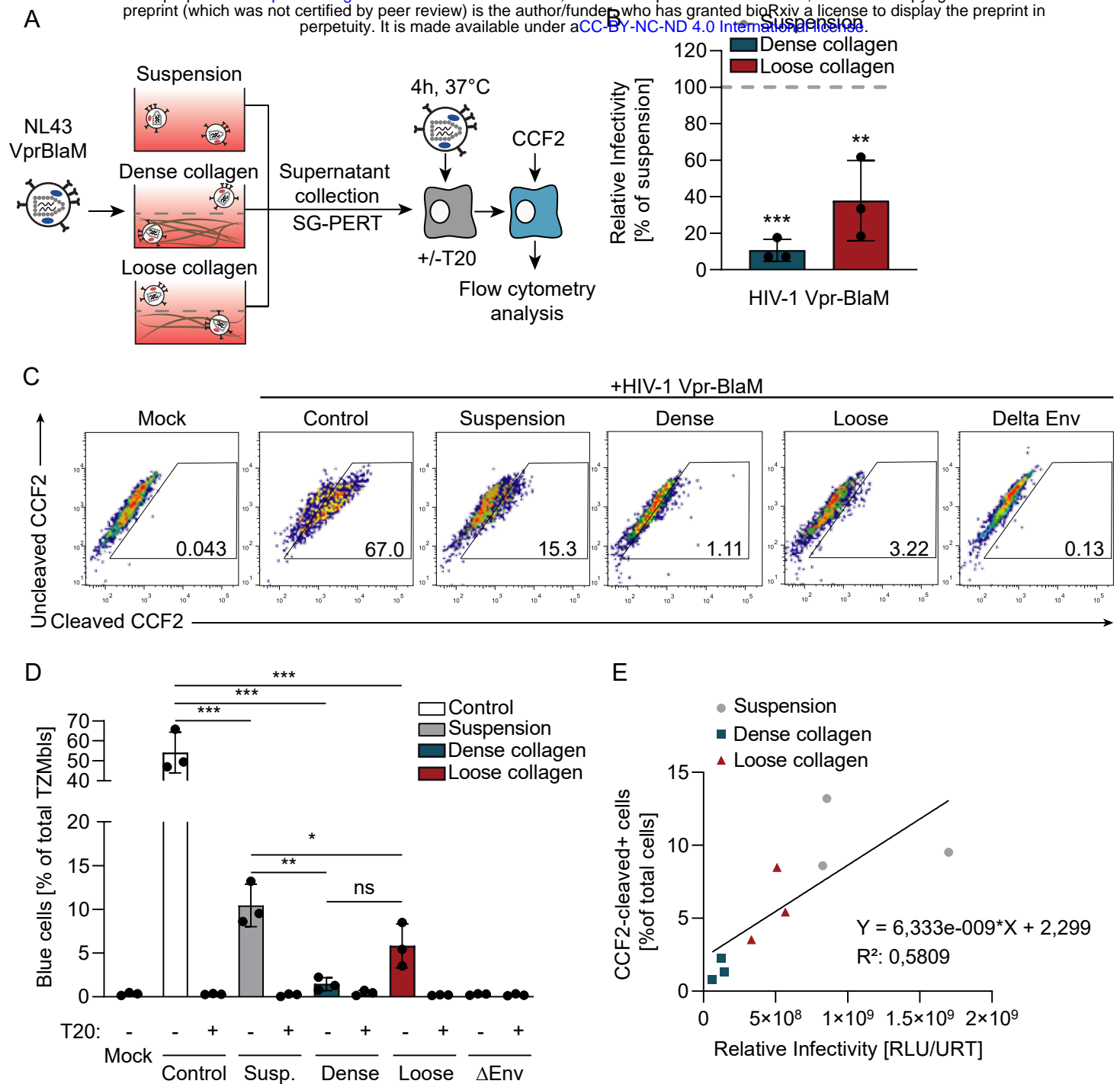
Fig. 4: Sid Ahmed et al, 2023
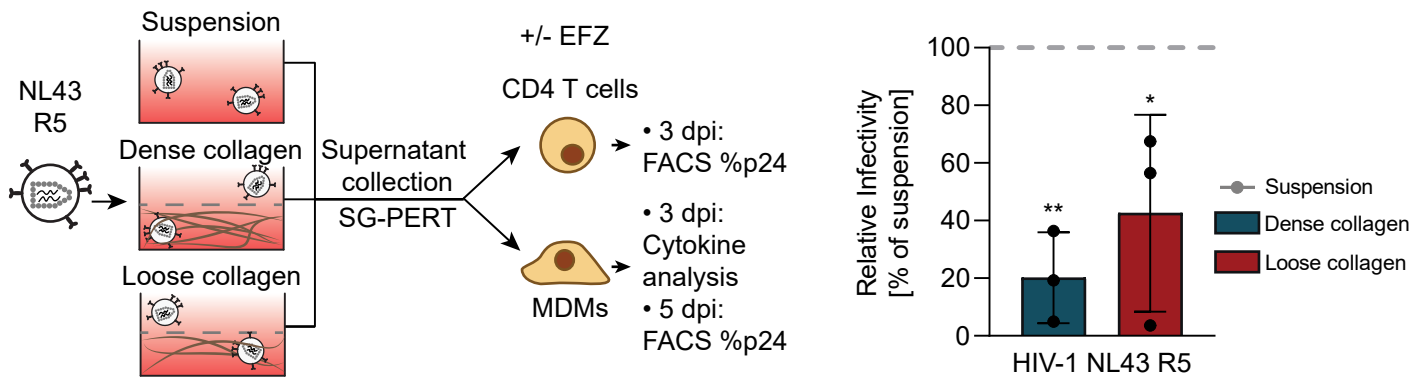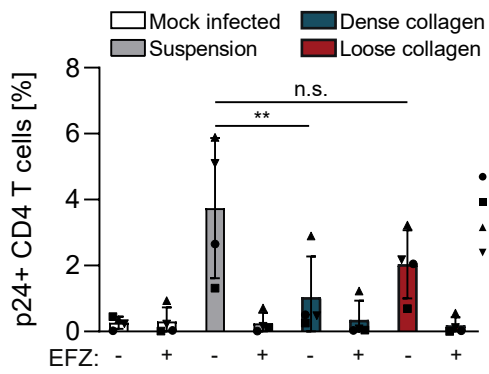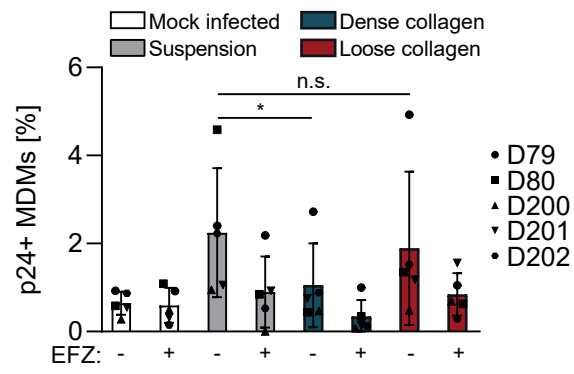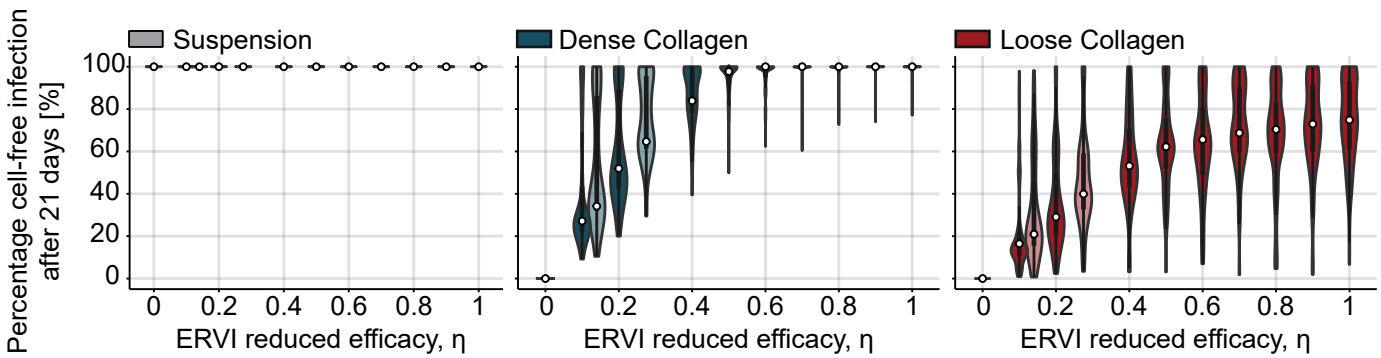
Fig. 5: Sid Ahmed et al, 2023

A

B

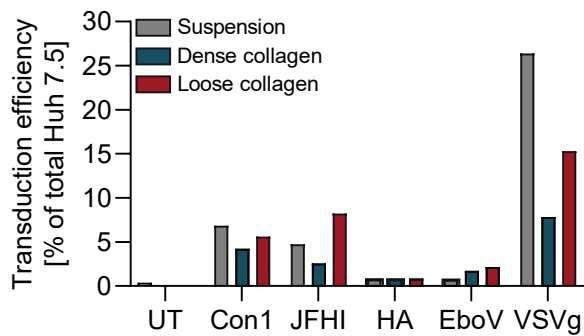

C
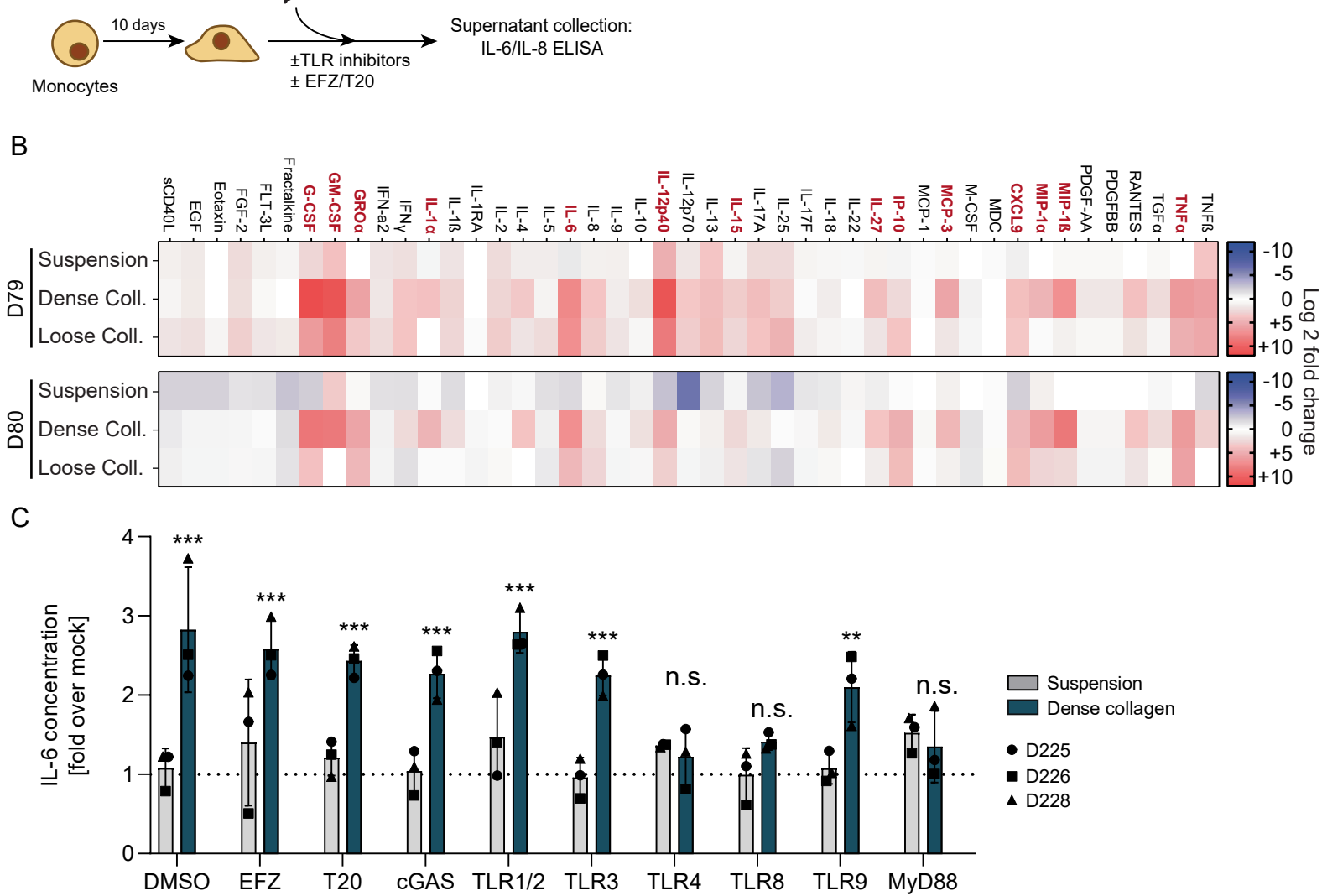
Fig. 6: Sid Ahmed et al, 2023

Fig. 7: Sid Ahmed et al, 2023

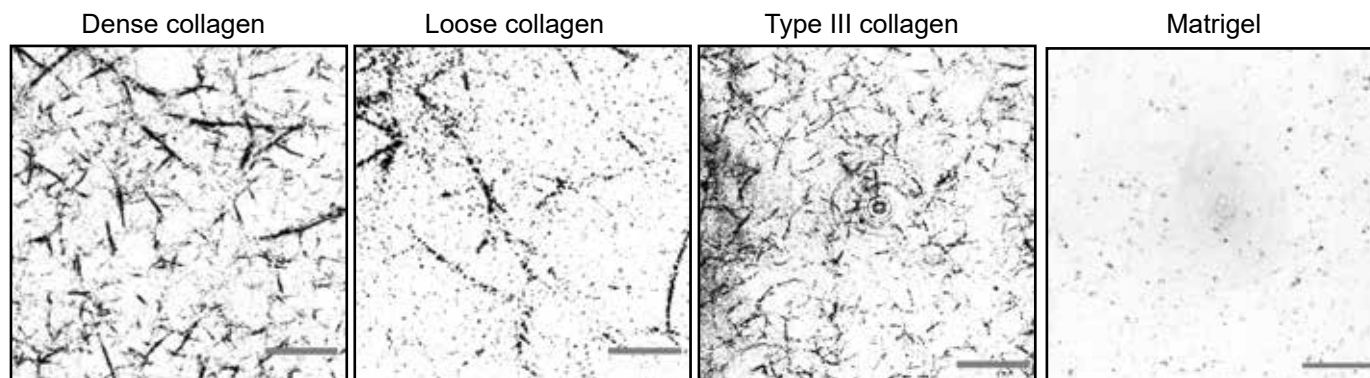Extended View 1: Sid Ahmed et al, 2023
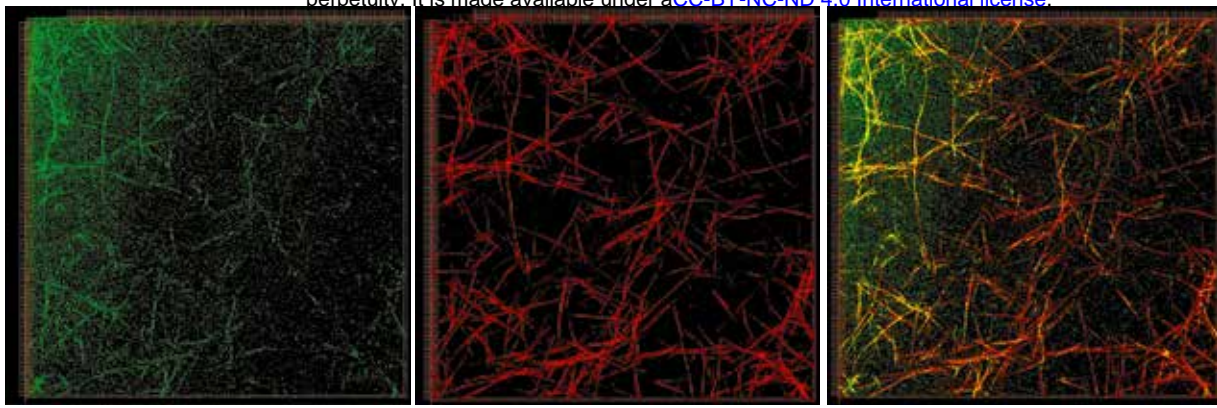
A

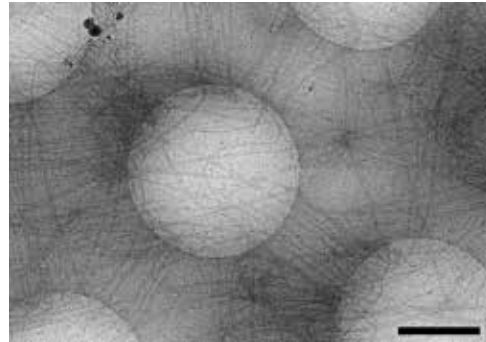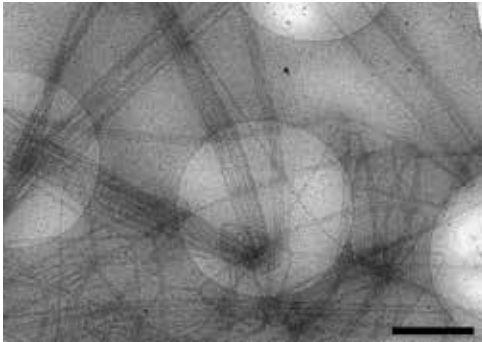488-channel　　　　　　　Autoreflection　　　　　　　Overlay
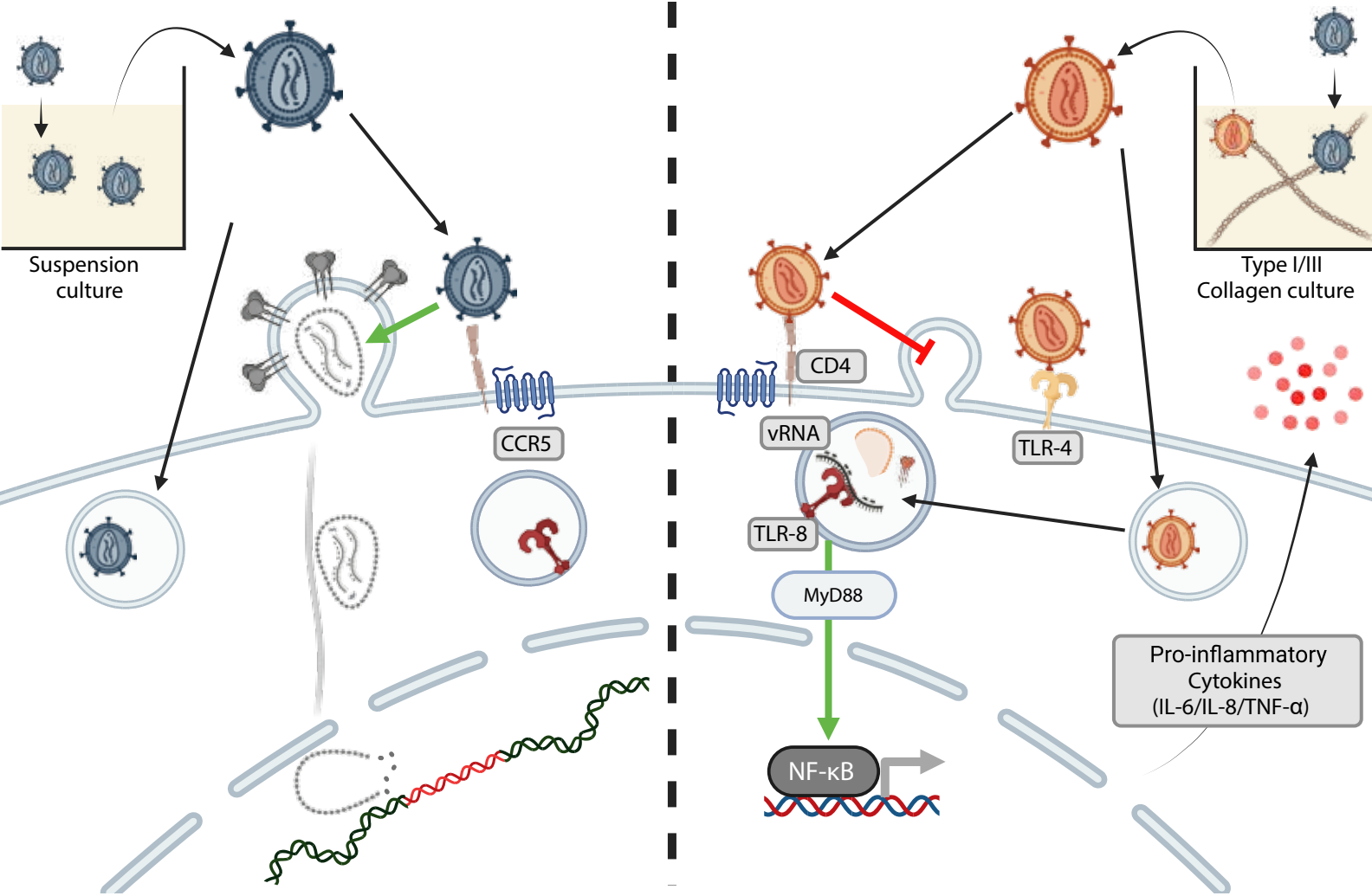
B

Dense collagen fibers　　　　　　　Loose collagen fibers
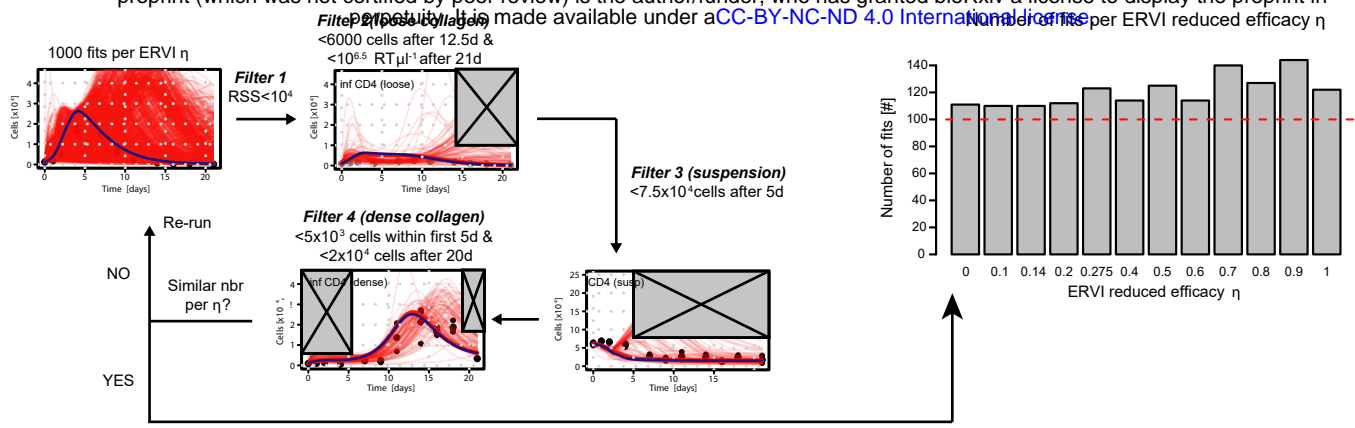

Extended View 2: Sid Ahmed et al, 2023

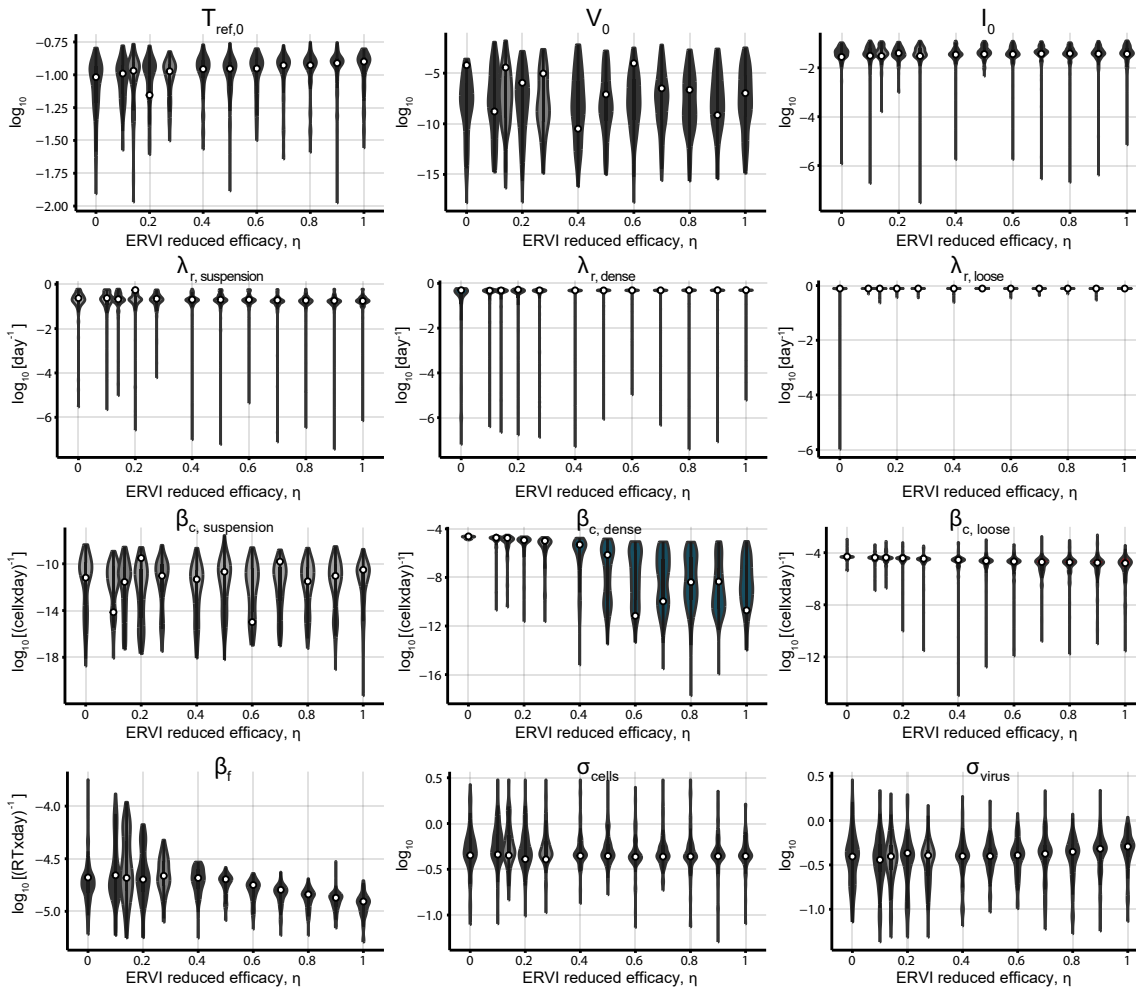Raw Data Virus segmentation Cell membrane segmentation
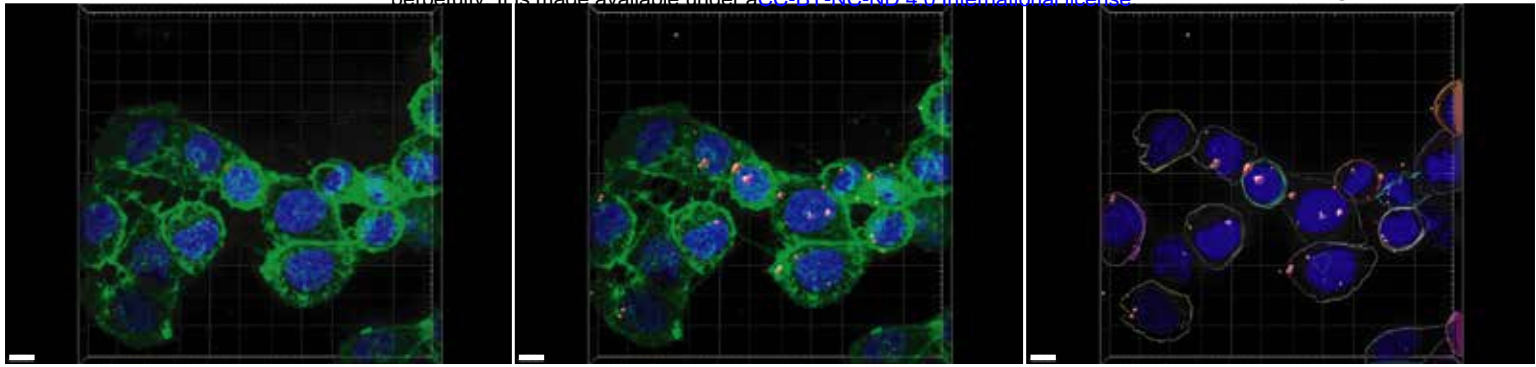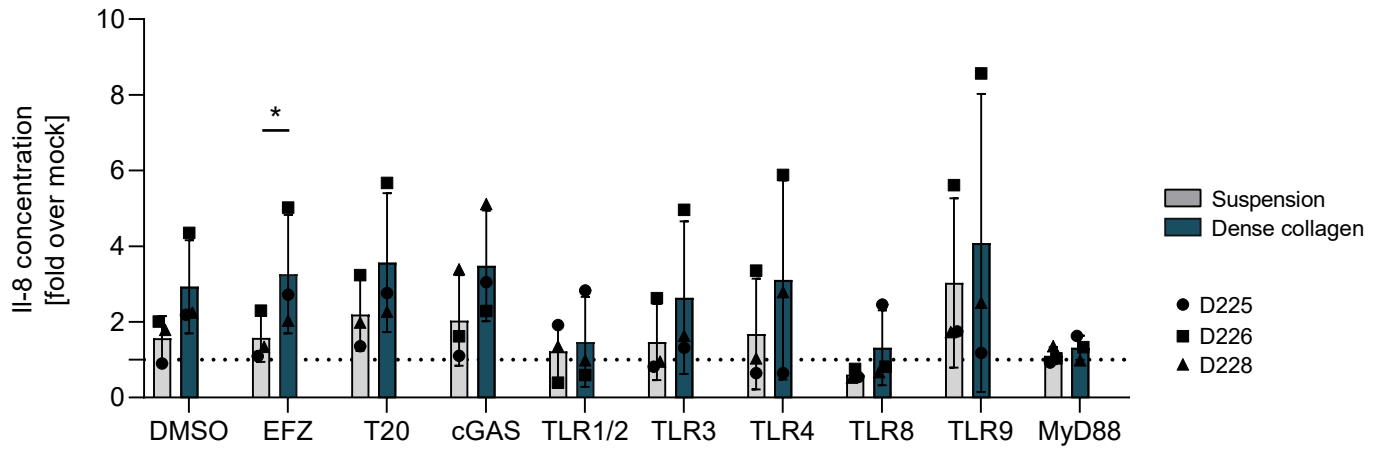
Extended View 3: Sid Ahmed et al, 2023

Extended View 4: Sid Ahmed et al, 2023

A

Extended View 5: Sid Ahmed et al, 2023